AIMS Mathematics, 11(10): 33105–33160.
DOI: 10.3934/math.20261298
Received: 27 August 2026
Revised: 01 October 2026
Accepted: 08 October 2026
Published: 13 October 2026

https://www.aimspress.com/journal/Math

Research article

A new Gompertz-type model with classical and Bayesian inference: applications to tax revenue and bank waiting-time data

Ayşe Metin KARAKAŞ[1], Fatma BULUT[2,*] and Murat KARAKAŞ[2]

[1] Department of Statistics, Faculty of Arts and Sciences, Bitlis Eren University, Bitlis, Turkey

[2] Department of Mathematics, Faculty of Arts and Sciences, Bitlis Eren University, Bitlis, Turkey

* **Correspondence:** Email: fbulut@beu.edu.tr.

Abstract: This study introduces the Kavya–Manoharan Cosine–Gompertz (KMCG) distribution, a parsimonious three-parameter Gompertz-type model. Its main mathematical properties, including the distribution, density, survival, hazard-rate, quantile, moment, and order-statistic functions, are derived. The KMCG hazard rate is strictly increasing for all admissible parameter values, restricting its use to settings where an increasing hazard structure is appropriate. Parameters are estimated by maximum likelihood and Bayesian methods using Markov chain Monte Carlo (MCMC) sampling. Monte Carlo results generally show improved estimation accuracy with increasing sample size. Applications to Egyptian monthly real tax revenue and bank-client waiting-time data are used to compare KMCG with several Gompertz-type models. For the first dataset, KMCG provides favorable information criteria, although the Inverse Gompertz model performs slightly better on some goodness-of-fit measures. For the second dataset, KMCG yields the smallest information criteria and goodness-of-fit statistics, with bootstrap p-values of 0.940, 0.976, and 0.952 for the Kolmogorov–Smirnov, Anderson–Darling, and Cramér–von Mises statistics, respectively. However, its AIC differs from that of the Transmuted Gompertz model by only about 0.129, indicating comparable performance. Bayesian estimates are broadly consistent with maximum likelihood results, while near-boundary estimates require cautious interpretation. Overall, KMCG provides a competitive alternative for positive-valued data with an increasing hazard structure, although its performance is data dependent.

Keywords: Kavya–Manoharan transformation; Cosine–Gompertz distribution; Gompertz distribution; hazard rate function; maximum likelihood estimation; Bayesian estimation; Markov chain Monte Carlo; Monte Carlo simulation
Mathematics Subject Classification: 62E10, 62E15, 62F15

1. Introduction

Continuous probability distributions are widely used to model positive and skewed observations in reliability, biomedical, engineering, actuarial, and economic applications [3, 6, 10]. Among them, the Gompertz distribution is a classical model characterized by an increasing hazard rate [11]. Its relatively restrictive distributional structure has motivated several extensions based on transmutation, power transformations, weighting, and generator mechanisms [1, 7–9, 14–17]. Recent studies have proposed several transformation-based extensions of classical lifetime distributions to obtain additional distributional shape control while retaining relatively parsimonious formulations. Among these, Kavya–Manoharan (KM)-based distributions have received attention in recent distributional modeling [2,5]. Recent studies have also developed Gompertz-type models and associated classical and Bayesian inferential procedures [12, 13]. These developments motivate the investigation of alternative Gompertz-type constructions that provide additional shape control without introducing an excessive number of parameters.

Motivated by this issue, we propose the three-parameter Kavya–Manoharan Cosine–Gompertz (KMCG) distribution by combining the cosine-G and KM transformations with the Gompertz baseline. The contribution is not merely the sequential application of two existing transformations; rather, the resulting construction is examined as a specific three-parameter model with an explicit distributional structure, increasing hazard behavior, classical and Bayesian inference, and finite-sample and real-data evaluation. Its three-parameter specification provides a relatively parsimonious alternative to more highly parameterized Gompertz extensions. However, fewer parameters do not by themselves guarantee better interpretability, numerical stability, or estimation efficiency, and these aspects are therefore evaluated empirically.

An important limitation of KMCG is that its hazard-rate function is strictly increasing for all admissible parameter values. Hence, the model is appropriate when an increasing event-occurrence or failure rate is substantively reasonable, but it is not designed to represent decreasing, bathtub-shaped, unimodal, or other non-monotone hazard patterns. Moreover, near-boundary estimates of some shape parameters may indicate weak identification and require careful inferential assessment. Thus, the proposed model is not claimed to be universally superior to existing Gompertz-type distributions.

Table 1 summarizes selected related Gompertz-type and transformation-based distributions and places the proposed KMCG model within the existing literature. The comparison highlights differences in construction, inferential approach, and application while avoiding a claim of general superiority.

Table 1. Comparison of selected related distributions with the proposed KMCG model.

Model	Reference	Construction	Inference	Main feature/application
Transmuted generalized Gompertz	[17]	Transmutation–Gompertz	Classical	Lifetime data
Alpha power Gompertz	[8]	Alpha-power transformation	Classical	Lifetime modeling
Shifted Gompertz–G	[9]	Gompertz–G generator	Classical	General distribution family
Gompertz extended generalized exponential	[7]	Gompertz generator	Classical	Lifetime applications
Kavya–Manoharan generalized exponential	[2]	KM transformation	Classical/Bayesian	Censored lifetime data
KM cosine inverse Rayleigh	[5]	KM + cosine transformation	Statistical inference	Radiation data
New Gompertz	[14]	Gompertz-type extension	Classical	Real-data applications
Novel Gompertz-type	[16]	Gompertz-type extension	Classical	Radiological/pharmacokinetic data
KMCG	**This study**	**KM + Cosine–Gompertz**	**MLE/Bayesian**	**Tax revenue/bank waiting times**

The parameters are estimated using maximum likelihood estimation (MLE) and Bayesian inference based on Markov chain Monte Carlo (MCMC) sampling. Their finite-sample behavior is investigated through Monte Carlo experiments. For empirical assessment, KMCG is compared with mathematically related Gompertz-type competitors using common information criteria, goodness-of-fit statistics, parametric-bootstrap p-values, graphical comparisons, and Bayesian diagnostics. The same comparison framework is used to evaluate relative performance rather than to assume superiority of the proposed model.

Two applications are considered: monthly real tax revenue in Egypt and bank-client waiting times. The bank waiting-time data permit a natural conditional event-occurrence interpretation, whereas the tax-revenue application is treated primarily as positive-data distributional modeling rather than as a literal lifetime mechanism. These applications therefore illustrate both the potential scope and the limitations of the proposed model.

The main contributions of this study are:

- to formulate the three-parameter KMCG distribution and establish its main distributional, survival, hazard, quantile, moment, and order-statistic properties;
- to characterize its strictly increasing hazard-rate structure and clarify the resulting scope of applicability;
- to develop MLE and Bayesian estimation procedures and examine their finite-sample behavior through simulation; and
- to assess its empirical performance against related Gompertz-type models while explicitly considering goodness of fit, parameter uncertainty, and near-boundary estimation.

The remainder of the paper is organized as follows. Section 2 introduces the KMCG distribution, Section 3 presents its main statistical properties, Section 4 develops the estimation procedures, Section 5 reports the simulation study, and Section 6 presents the real-data applications. Section 7 concludes the paper.

2. The Kavya–Manoharan Cosine–Gompertz distribution

This section introduces the Kavya–Manoharan Cosine–Gompertz (KMCG) distribution by combining the Gompertz baseline with the cosine-G and Kavya–Manoharan transformations. The construction is presented sequentially to make the mathematical structure of the proposed three-parameter distribution explicit.

2.1. The Gompertz distribution

We begin with the Gompertz distribution as the baseline model. For $\alpha, \lambda > 0$, its cumulative distribution function (CDF) is given by

$$G(x) = 1 - \exp\left[-\frac{\lambda}{\alpha}(e^{\alpha x} - 1)\right], \qquad x > 0, \tag{2.1}$$

and its probability density function (PDF) is

$$g(x) = \lambda e^{\alpha x} \exp\left[-\frac{\lambda}{\alpha}(e^{\alpha x} - 1)\right], \qquad x > 0. \tag{2.2}$$

For convenience, define

$$T(x) = \frac{\lambda}{\alpha}\left(e^{\alpha x} - 1\right). \tag{2.3}$$

Then, Eqs (2.1) and (2.2) can be written as

$$G(x) = 1 - e^{-T(x)} \tag{2.4}$$

and

$$g(x) = \lambda e^{\alpha x} e^{-T(x)} \tag{2.5}$$

where $\alpha > 0$ is the shape parameter controlling the rate of increase of the Gompertz hazard function, and $\lambda > 0$ is the rate parameter determining its initial value, $h(0) = \lambda$.

2.2. The Cosine–G transformation

For a baseline distribution with CDF $G(x)$ and PDF $g(x)$, the Cosine-G transformation is defined by the CDF

$$R(x) = 1 - \cos\left(\frac{\pi}{2}G(x)\right). \tag{2.6}$$

For the Gompertz baseline, substituting the CDF given in Eq (2.1) into Eq (2.6) yields

$$R(x) = 1 - \cos\left[\frac{\pi}{2}\left\{1 - \exp\left[-\frac{\lambda}{\alpha}\left(e^{\alpha x} - 1\right)\right]\right\}\right]. \tag{2.7}$$

The corresponding PDF is obtained by differentiating Eq (2.6) with respect to x. Thus,

$$r(x) = \frac{\pi}{2}\, g(x) \sin\left(\frac{\pi}{2}G(x)\right). \tag{2.8}$$

To obtain the Cosine–Gompertz density, we substitute the Gompertz CDF and PDF into the general Cosine–G density in Eq (2.8). For the Gompertz baseline,

$$G(x) = 1 - \exp\left[-\frac{\lambda}{\alpha}\left(e^{\alpha x} - 1\right)\right] \tag{2.9}$$

and

$$g(x) = \lambda e^{\alpha x} \exp\left[-\frac{\lambda}{\alpha}\left(e^{\alpha x} - 1\right)\right], \qquad x > 0, \quad \alpha, \lambda > 0. \tag{2.10}$$

Substituting these expressions for $G(x)$ and $g(x)$ into Eq (2.8) gives

$$\begin{aligned} r(x) = \frac{\pi}{2}\lambda e^{\alpha x} \exp\left[-\frac{\lambda}{\alpha}\left(e^{\alpha x} - 1\right)\right] \\ \times \sin\left[\frac{\pi}{2}\left\{1 - \exp\left[-\frac{\lambda}{\alpha}\left(e^{\alpha x} - 1\right)\right]\right\}\right], \qquad x > 0. \end{aligned} \tag{2.11}$$

Collecting the constant and exponential terms, the Cosine–Gompertz density can equivalently be written as

$$f_{\mathrm{CG}}(x) = \frac{\pi\lambda}{2} e^{\alpha x} \exp\left[-\frac{\lambda}{\alpha}\left(e^{\alpha x} - 1\right)\right] \sin\left[\frac{\pi}{2}\left\{1 - \exp\left[-\frac{\lambda}{\alpha}\left(e^{\alpha x} - 1\right)\right]\right\}\right], \quad x > 0. \tag{2.12}$$

Hence, $R(x)$ and $r(x)$ are respectively the CDF and PDF of the Cosine–Gompertz distribution obtained from the Gompertz baseline. For consistency with the subsequent Kavya–Manoharan transformation, we use $r(x)$ to denote the Cosine–Gompertz PDF throughout the remainder of the paper.

2.3. The Kavya–Manoharan transformation

The Kavya–Manoharan transformation is subsequently applied to the Cosine–Gompertz CDF $R(x)$. For $\beta > 0$, the transformation is defined by

$$F(x) = \frac{e^{\beta R(x)} - 1}{e^{\beta} - 1}. \tag{2.13}$$

Differentiating Eq (2.13) with respect to x gives the corresponding density

$$f(x) = \frac{\beta e^{\beta R(x)}}{e^{\beta} - 1} r(x), \tag{2.14}$$

where $\beta > 0$ is the additional shape parameter introduced by the Kavya–Manoharan generator.

2.4. The KMCG distribution

Combining the Gompertz baseline with the Cosine-G and Kavya–Manoharan transformations yields the proposed Kavya–Manoharan Cosine–Gompertz (KMCG) distribution. For $\alpha, \beta, \lambda > 0$, its CDF is

$$F_{\mathrm{KMCG}}(x) = \frac{e^{\beta R(x)} - 1}{e^{\beta} - 1}, \qquad x > 0, \tag{2.15}$$

where $R(x)$ is given by Eq (2.7). Using Eq (2.14), the PDF of the KMCG distribution can be expressed compactly as

$$f_{\mathrm{KMCG}}(x) = \frac{\beta e^{\beta R(x)}}{e^{\beta} - 1} r(x), \qquad x > 0. \tag{2.16}$$

Substituting Eq (2.11) into Eq (2.16), we obtain

$$\begin{aligned} f_{\mathrm{KMCG}}(x) = {} & \frac{\beta \pi \lambda e^{\alpha x}}{2(e^{\beta} - 1)} \exp\left[-\frac{\lambda}{\alpha}\left(e^{\alpha x} - 1\right)\right] \\ & \times \sin\left[\frac{\pi}{2}\left\{1 - \exp\left[-\frac{\lambda}{\alpha}\left(e^{\alpha x} - 1\right)\right]\right\}\right] \\ & \times \exp\left\{\beta\left[1 - \cos\left(\frac{\pi}{2}\left\{1 - \exp\left[-\frac{\lambda}{\alpha}\left(e^{\alpha x} - 1\right)\right]\right\}\right)\right]\right\}, \qquad x > 0. \end{aligned} \tag{2.17}$$

Equations (2.15) and (2.17) define the proposed three-parameter KMCG distribution. The construction proceeds from the Gompertz baseline through the cosine-G transformation, followed by the Kavya–Manoharan transformation. Thus, the resulting model provides a distinct three-parameter distributional specification with explicit CDF and PDF forms that can be used for likelihood-based and Bayesian inference. Its statistical flexibility should be interpreted within the class of distributions having an increasing hazard rate, as established in the subsequent analysis.

Interpretation of the parameters. The parameters α, β, and λ are shape and rate parameters rather than pure location or scale parameters. In the Gompertz baseline,

$$T(x) = \frac{\lambda}{\alpha}(e^{\alpha x} - 1) = \lambda \int_0^x e^{\alpha t}\, dt.$$

Thus, for fixed $x > 0$, increasing either λ or α increases $T(x)$ and the resulting KMCG cumulative distribution function. Holding the other parameters fixed, either change therefore shifts probability towards smaller values of x. The parameter λ also controls the baseline hazard level, whereas α governs its exponential rate of increase. The parameter β acts through the Kavya–Manoharan transformation

$$F_{\mathrm{KMCG}}(x) = \frac{e^{\beta R(x)} - 1}{e^{\beta} - 1}, \qquad R(x) = 1 - \cos\left[\frac{\pi}{2}\left\{1 - e^{-T(x)}\right\}\right].$$

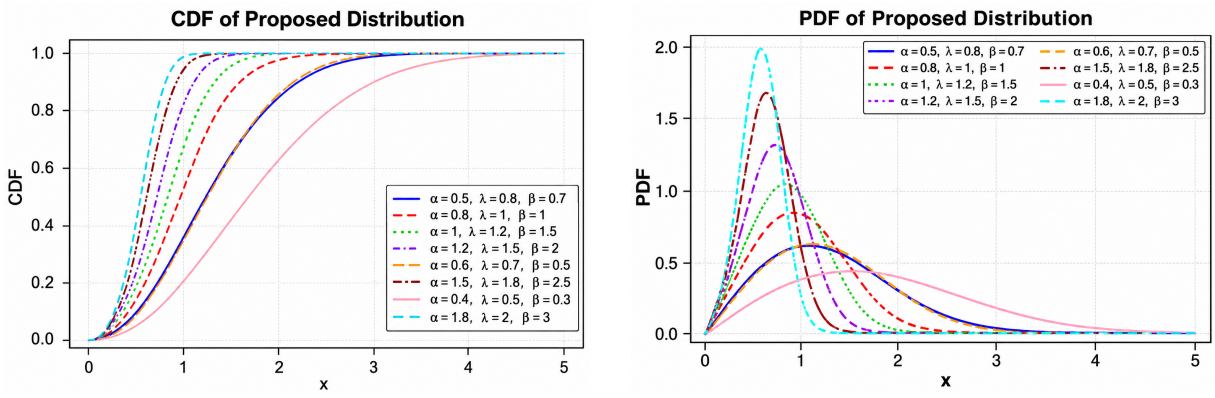
For $0 < R(x) < 1$, increasing β decreases $F_{\mathrm{KMCG}}(x)$; hence, with α and λ fixed, it shifts probability towards larger values of x. Parameter changes can also alter the density shape and numerical measures such as skewness, but these effects depend on the joint parameter configuration and are not described here as universal monotone changes in skewness. The right-tail hazard satisfies

$$h_{\mathrm{KMCG}}(x) \sim \lambda e^{\alpha x}, \qquad x \to \infty.$$

Consequently, α determines the asymptotic exponential growth rate, while λ determines its multiplicative level. The parameter β affects the hazard at finite values of x, but not this leading right-tail growth rate.

2.5. *Behavior of the KMCG distribution*

Figure 1 illustrates the behavior of the CDF and PDF of the proposed KMCG distribution for several combinations of α, λ, and β.



(a) CDF plots for different parameter values.

(b) PDF plots for different parameter values.

Figure 1. Behavior of the proposed Kavya–Manoharan Cosine Gompertz (KMCG) distribution for different combinations of α, λ, and β: (a) cumulative distribution function and (b) probability density function.

Figure 1 illustrates the flexibility of the KMCG distribution under different parameter combinations. Panel (a) shows that α, λ, and β affect the rate at which the CDF approaches one, while Panel (b) demonstrates their influence on the location, concentration, skewness, and tail behavior of the density. These results illustrate the ability of the KMCG distribution to accommodate different shapes of positively skewed lifetime data. Recall that

$$R(x) = 1 - \cos\left(\frac{\pi}{2}G(x)\right),$$

where

$$G(x) = 1 - \exp\left[-\frac{\lambda}{\alpha}\left(e^{\alpha x} - 1\right)\right].$$

For $\alpha, \beta, \lambda > 0$, the proposed density can be written as

$$f_{\mathrm{KMCG}}(x) = \frac{\beta}{e^{\beta} - 1} e^{\beta R(x)} R'(x).$$

Since

$$G(0) = 0, \qquad \lim_{x\to\infty} G(x) = 1,$$

we have

$$R(0) = 0, \qquad \lim_{x\to\infty} R(x) = 1.$$

Therefore, using the substitution $u = R(x)$, we obtain

$$\begin{aligned}
\int_0^{\infty} f_{\mathrm{KMCG}}(x)\, dx &= \frac{\beta}{e^{\beta} - 1} \int_0^{\infty} e^{\beta R(x)} R'(x)\, dx \\
&= \frac{\beta}{e^{\beta} - 1} \int_0^{1} e^{\beta u}\, du \\
&= \frac{\beta}{e^{\beta} - 1} \left[\frac{e^{\beta u}}{\beta}\right]_0^{1} \\
&= 1.
\end{aligned}$$

Thus, $f_{\mathrm{KMCG}}(x)$ is a properly normalized probability density on $(0, \infty)$.

2.6. *Survival function*

The survival function is defined as

$$S(x) = 1 - F_{\mathrm{KMCG}}(x). \tag{2.18}$$

Therefore,

$$S(x) = \frac{1}{e^{\beta} - 1}\left[e^{\beta} - \exp\left\{\beta\left[1 - \cos\left(\frac{\pi}{2}\left\{1 - \exp\left[-\frac{\lambda}{\alpha}\left(e^{\alpha x} - 1\right)\right]\right\}\right)\right]\right\}\right]. \tag{2.19}$$

Figure 2 illustrates the survival function of the proposed KMCG distribution for selected parameter values.

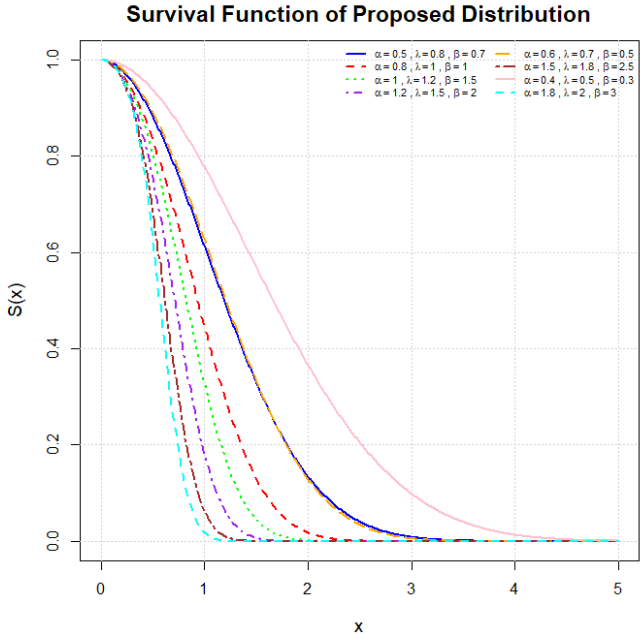


Figure 2. Survival function plots of the proposed Kavya–Manoharan Cosine Gompertz distribution for different parameter values.

2.7. Hazard-rate properties

Let

$$T(x) = \frac{\lambda}{\alpha}\left(e^{\alpha x} - 1\right), \qquad \delta(x) = \frac{\pi}{2}e^{-T(x)}. \tag{2.20}$$

Using

$$h(x) = \frac{f_{\mathrm{KMCG}}(x)}{S(x)},$$

the hazard-rate function of the proposed distribution can be expressed as

$$h(x) = \frac{\beta\pi\lambda e^{\alpha x}}{2}\,\frac{e^{-T(x)}\cos\delta(x)}{\exp\{\beta\sin\delta(x)\} - 1}, \qquad x > 0. \tag{2.21}$$

Since

$$\lambda e^{\alpha x} = \lambda + \alpha T(x), \qquad e^{-T(x)} = \frac{2\delta(x)}{\pi},$$

an equivalent representation is

$$h(x) = \frac{\beta\{\lambda + \alpha T(x)\}\delta(x)\cos\delta(x)}{\exp\{\beta\sin\delta(x)\} - 1}. \tag{2.22}$$

Equation (2.22) is particularly convenient for numerical evaluation because it avoids subtracting nearly equal exponential terms in the right tail.

Proposition 2.1. *For $\alpha, \lambda, \beta > 0$, the hazard-rate function satisfies*

$$h(x) \sim \frac{\beta\pi^2\lambda^2}{4(e^{\beta} - 1)}x, \quad x \to 0^+, \tag{2.23}$$

$$h(x) \sim \lambda e^{\alpha x}, \quad x \to \infty. \tag{2.24}$$

Consequently,

$$\lim_{x\to 0^+} h(x) = 0, \qquad \lim_{x\to\infty} h(x) = \infty.$$

Proof. As $x \to 0^+$,

$$T(x) \sim \lambda x$$

and

$$1 - e^{-T(x)} \sim \lambda x.$$

Therefore,

$$\sin\left\{\frac{\pi}{2}\left(1 - e^{-T(x)}\right)\right\} \sim \frac{\pi\lambda x}{2},$$

whereas

$$\cos\left\{\frac{\pi}{2}\left(1 - e^{-T(x)}\right)\right\} \to 1.$$

Substitution into the hazard-rate function yields

$$h(x) \sim \frac{\beta\pi^2\lambda^2}{4(e^\beta - 1)}x.$$

For $x \to \infty$, we have $T(x) \to \infty$ and $\delta(x) \to 0$. Consequently,

$$\sin\delta(x) \sim \delta(x), \qquad \cos\delta(x) \to 1,$$

and

$$\exp\{\beta\sin\delta(x)\} - 1 \sim \beta\delta(x).$$

It follows from Eq (2.22) that

$$h(x) \sim \lambda + \alpha T(x) = \lambda e^{\alpha x}.$$

This completes the proof. □

Proposition 2.2. *For every $\alpha, \lambda, \beta > 0$, the hazard-rate function is strictly increasing on* $(0, \infty)$.

Proof. Since

$$T'(x) = \lambda e^{\alpha x} = \lambda + \alpha T(x) > 0,$$

the derivatives of $h(x)$ with respect to x and T have the same sign. Define

$$z = \beta\sin\delta$$

and

$$A(z) = \frac{z}{1 - e^{-z}}.$$

Differentiating the logarithm of Eq (2.22) with respect to T gives

$$\frac{\mathrm{d}}{\mathrm{d}T}\log h = \frac{\alpha}{\lambda + \alpha T} - 1 + \delta\tan\delta + A(z)\delta\cot\delta. \tag{2.25}$$

For $z > 0$, the inequality $1 - e^{-z} < z$ implies that

$$A(z) > 1.$$

Moreover, since $0 < \delta < \pi/2$,

$$\delta \tan \delta + \delta \cot \delta = \frac{\delta}{\sin \delta \cos \delta} > 1. \tag{2.26}$$

It follows that

$$\frac{\mathrm{d}}{\mathrm{d}T} \log h > \frac{\alpha}{\lambda + \alpha T} - 1 + \delta \tan \delta + \delta \cot \delta \tag{2.27}$$

$$> \frac{\alpha}{\lambda + \alpha T} > 0. \tag{2.28}$$

Therefore, $h'(x) > 0$ for every $x > 0$, proving that the distribution has a strictly increasing hazard rate. □

Asymptotic behavior of the hazard rate. To isolate the contribution of the Gompertz component, let

$$s(x) = \exp\left[-\frac{\lambda}{\alpha}(e^{\alpha x} - 1)\right], \qquad u(x) = \frac{\pi}{2} s(x), \qquad v(x) = \beta \sin(u(x)).$$

The KMCG hazard rate admits the factorization

$$h_{\mathrm{KMCG}}(x) = \underbrace{\lambda e^{\alpha x}}_{h_{\mathrm{G}}(x)} [u(x) \cot u(x)] \left[\frac{v(x)}{e^{v(x)} - 1}\right], \tag{2.29}$$

where $h_{\mathrm{G}}(x) = \lambda e^{\alpha x}$ is the hazard rate of the Gompertz baseline. As $x \to \infty$, we have $s(x) \to 0$, and hence $u(x) \to 0$ and $v(x) \to 0$. Since

$$\lim_{u \to 0} u \cot u = 1$$

and

$$\lim_{v \to 0} \frac{v}{e^v - 1} = 1,$$

it follows that

$$\lim_{x \to \infty} \frac{h_{\mathrm{KMCG}}(x)}{h_{\mathrm{G}}(x)} = 1. \tag{2.30}$$

Therefore,

$$h_{\mathrm{KMCG}}(x) \sim \lambda e^{\alpha x}, \qquad (x \to \infty).$$

The exponential acceleration of the KMCG hazard in the right tail is thus governed by the Gompertz component. The cosine and Kavya–Manoharan transformations modify the hazard at finite values of x, while their multiplicative correction approaches one in the right tail.

Interpretation of the hazard-rate parameters

The preceding results establish that the proposed distribution belongs to the increasing-failure-rate (IFR) class for every admissible parameter combination. The parameters substantially modify the level and curvature of the hazard function, although they do not change its monotonicity class. The parameter β primarily controls the early- and intermediate-time hazard levels. In particular, the initial slope is

$$h'(0^+) = \frac{\beta\pi^2\lambda^2}{4(e^\beta - 1)}. \tag{2.31}$$

Since $\beta/(e^\beta - 1)$ decreases with β, larger values of β produce a lower initial hazard rate. However, β does not appear in the leading right-tail term. The parameter α determines the exponential acceleration of the hazard in the right tail, whereas λ affects both the initial slope and the asymptotic hazard level. Specifically,

$$h(x) \sim \lambda e^{\alpha x}, \qquad x \to \infty. \tag{2.32}$$

Thus, λ acts as a hazard-level parameter, while α determines the rate at which the hazard grows for large values of x.

Figure 3 provides a graphical illustration of the theoretical hazard-rate results. Panel (a) shows that varying β mainly affects the hazard level at small and intermediate values of x, while the curves become increasingly similar in the right tail. This behavior agrees with the asymptotic result $h(x) \sim \lambda e^{\alpha x}$, which is independent of β. Panel (b) demonstrates the strong influence of α on the growth rate of the hazard function. Larger values of α produce a much more rapid increase in the hazard for large x, confirming that α governs the exponential acceleration of the right-tail hazard. Panel (c) indicates that increasing λ raises the overall hazard level and also increases its initial slope, consistently with

$$h'(0^+) = \frac{\beta\pi^2\lambda^2}{4(e^\beta - 1)}.$$

Finally, Panel (d) shows that

$$\frac{\mathrm{d}}{\mathrm{d}x} \log h(x) > 0$$

for the displayed parameter combinations. Hence, the numerical results support the analytical result that $h'(x) > 0$ for $x > 0$. Taken together, the four panels confirm that the proposed distribution exhibits a strictly increasing failure rate, while α, λ, and β provide substantial control over the level and curvature of the hazard function. Figure 3 provides a graphical illustration of the theoretical hazard-rate results. Panel (a) shows that varying β mainly affects the hazard level at small and intermediate values of x, while the curves become increasingly similar in the right tail. This behavior agrees with the asymptotic result $h(x) \sim \lambda e^{\alpha x}$, which is independent of β. Panel (b) demonstrates the strong influence of α on the growth rate of the hazard function. Larger values of α produce a much more rapid increase in the hazard for large x, confirming that α governs the exponential acceleration of the right-tail hazard. Panel (c) indicates that increasing λ raises the overall hazard level and also increases its initial slope, consistently with

$$h'(0^+) = \frac{\beta\pi^2\lambda^2}{4(e^\beta - 1)}.$$

Finally, Panel (d) shows that

$$\frac{\mathrm{d}}{\mathrm{d}x} \log h(x) > 0$$

for the displayed parameter combinations. Hence, the numerical results support the analytical result that $h'(x) > 0$ for $x > 0$. Taken together, the four panels confirm that the proposed distribution exhibits a strictly increasing failure rate, while α, λ, and β provide substantial control over the level and curvature of the hazard function.

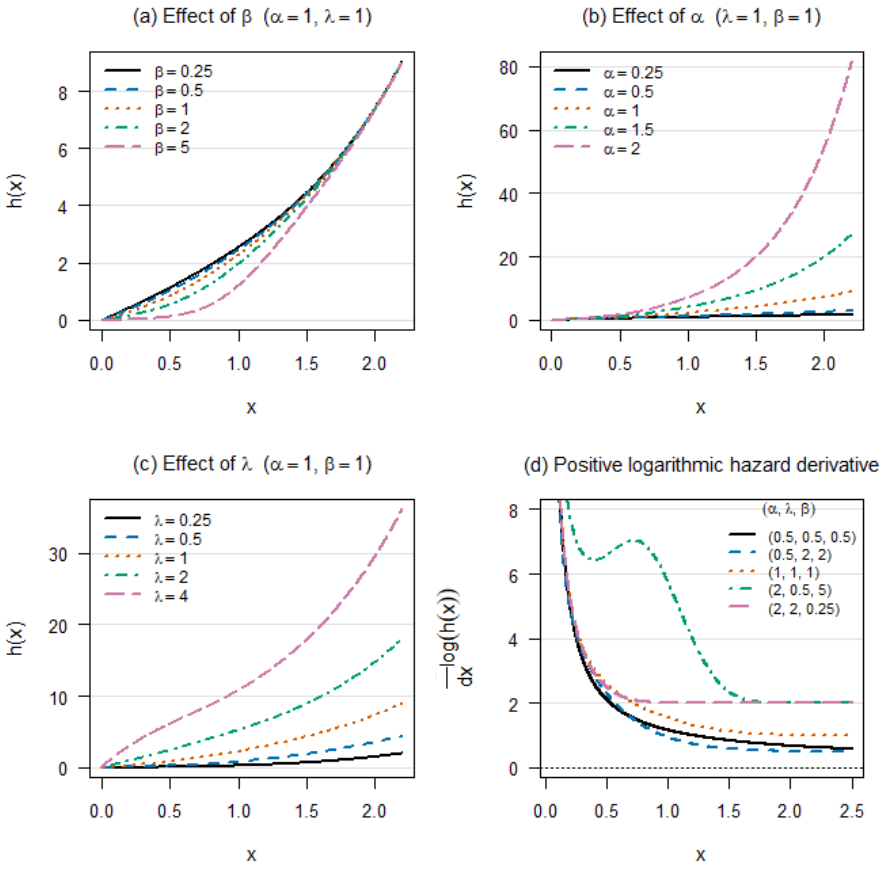


Figure 3. Hazard-rate behavior of the proposed distribution under different parameter configurations: (a) effect of β for $\alpha = 1$ and $\lambda = 1$; (b) effect of α for $\lambda = 1$ and $\beta = 1$; (c) effect of λ for $\alpha = 1$ and $\beta = 1$; and (d) the derivative of the logarithmic hazard function for selected parameter combinations. The results illustrate the strictly increasing hazard-rate behavior of the proposed distribution.

The preceding result establishes that the KMCG distribution belongs to the increasing-failure-rate class for all $\alpha, \beta, \lambda > 0$. The parameter configurations in Figure 3 illustrate different magnitudes and rates of increase, while preserving the increasing hazard shape. Accordingly, the flexibility of the model should be understood in terms of its distributional shape and variation within the class of increasing hazard rates. The KMCG distribution cannot generate a decreasing, bathtub-shaped, unimodal, or other non-monotone hazard rate under the stated parameter restrictions. Its use is therefore most appropriate when an increasing hazard is substantively plausible for the data being analyzed. The proposed model allows variation in distributional shape and in the rate at which the hazard increases, while retaining a strictly increasing hazard function.

2.8. Quantile function

The quantile function of the KMCG distribution is obtained by solving $F(x) = u$, $0 < u < 1$. It is given by

$$Q(u) = \frac{1}{\alpha} \ln \left\{ 1 - \frac{\alpha}{\lambda} \ln \left[1 - \frac{2}{\pi} \arccos\left(C(u)\right) \right] \right\}, \tag{2.33}$$

where

$$C(u) = 1 - \frac{1}{\beta} \ln \left[1 + u(e^{\beta} - 1) \right]. \tag{2.34}$$

This closed-form expression facilitates random variate generation and the computation of distributional percentiles. Table 2 presents the quantile function values of the proposed KMCG distribution for selected combinations of the parameters (α, β, λ). For all parameter combinations, the quantile values increase monotonically as the probability level q increases from 0.1 to 0.9, as expected for a valid quantile function. The table also illustrates the effect of different parameter configurations on the distributional quantiles. Noticeable differences among the reported quantiles indicate that variations in (α, β, λ) can substantially affect the location and shape of the resulting distribution. In particular, the parameter combinations produce different rates of increase across the quantile levels, demonstrating the flexibility of the proposed model in representing different distributional behaviors. These results also provide useful numerical evidence for the effect of the model parameters on the quantile function.

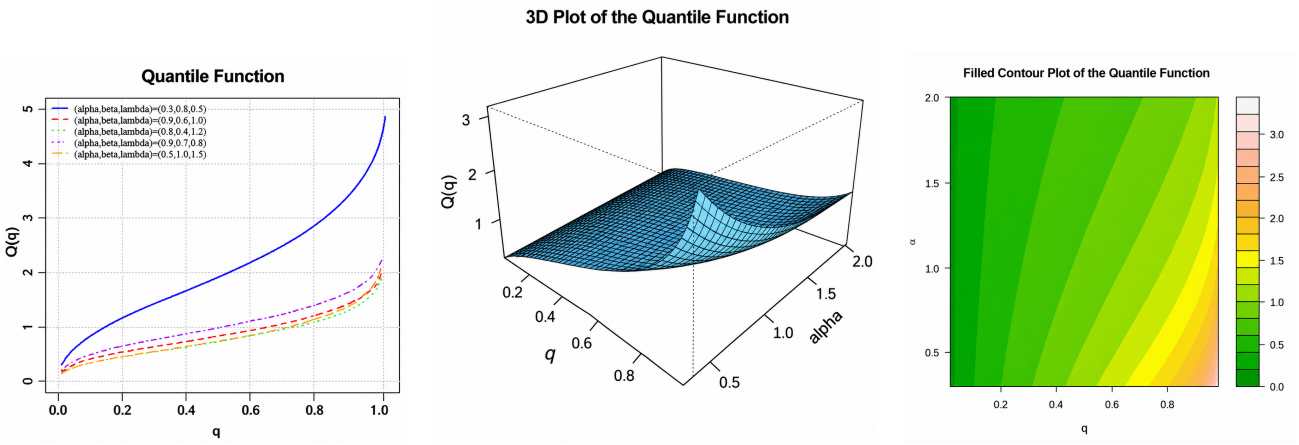
Table 2. Quantile function values for selected parameter combinations (α, β, λ).

q	$(\alpha, \beta, \lambda) = (0.3, 0.8, 0.5)$	$(\alpha, \beta, \lambda) = (0.9, 0.6, 1.0)$	$(\alpha, \beta, \lambda) = (0.8, 0.4, 1.2)$	$(\alpha, \beta, \lambda) = (0.9, 0.7, 0.8)$	$(\alpha, \beta, \lambda) = (0.5, 1.0, 1.5)$
0.1	0.757800	0.342437	0.281271	0.424016	0.280480
0.2	1.111016	0.494594	0.413941	0.603221	0.418172
0.3	1.407616	0.619937	0.526931	0.747291	0.536606
0.4	1.684137	0.735090	0.633597	0.877196	0.649273
0.5	1.958612	0.847905	0.740609	1.002489	0.763270
0.6	2.246002	0.964533	0.853653	1.130245	0.884973
0.7	2.565285	1.092395	0.980139	1.268548	1.023029
0.8	2.951242	1.244670	1.133828	1.431259	1.193937
0.9	3.501772	1.457811	1.353561	1.656123	1.445302

Figure 4 illustrates the behavior of the quantile function of the proposed KMCG distribution from different graphical perspectives. The parameter space of the proposed KMCG distribution is

$$\alpha > 0, \qquad \lambda > 0, \qquad \beta > 0. \tag{2.35}$$

Here, α is the Gompertz shape parameter, λ is the scale/risk parameter, and β is the Kavya–Manoharan shape parameter. The proposed model is capable of exhibiting a wide variety of density and hazard-rate shapes. Depending on the parameter values, the hazard rate may display increasing, decreasing, bathtub-shaped, or upside-down bathtub-shaped behavior, while the density function can accommodate different degrees of right skewness and tail behavior.



(a) Quantile function plots for different combinations of α, β, and λ.

(b) Three-dimensional surface plot of the quantile function as a function of q and α.

(c) Filled contour plot of the quantile function as a function of q and α.

Figure 4. Graphical representations of the quantile function of the proposed Kavya–Manoharan Cosine Gompertz (KMCG) distribution: (a) quantile curves, (b) three-dimensional surface, and (c) filled contour plot.

3. Some statistical properties

This section presents some statistical properties of the KMCG distribution, including its moments and related measures. These properties provide useful information about the distributional characteristics of the proposed model.

3.1. Moments and related measures

Let X follow the Kavya–Manoharan Cosine–Gompertz (KMCG) distribution with parameters $\alpha, \lambda, \beta > 0$, whose probability density function is

$$\begin{aligned} f(x;\alpha,\lambda,\beta) = {} & \frac{\beta\pi\lambda}{2(e^{\beta}-1)} e^{\alpha x} \exp\left[-\frac{\lambda}{\alpha}(e^{\alpha x}-1)\right] \\ & \times \sin\left[\frac{\pi}{2}\left\{1-\exp\left[-\frac{\lambda}{\alpha}(e^{\alpha x}-1)\right]\right\}\right] \\ & \times \exp\left\{\beta\left[1-\cos\left(\frac{\pi}{2}\left\{1-\exp\left[-\frac{\lambda}{\alpha}(e^{\alpha x}-1)\right]\right\}\right)\right]\right\}, \qquad x>0. \end{aligned} \tag{3.1}$$

The rth raw moment of X is defined by

$$\mu'_r = E(X^r) = \int_0^{\infty} x^r f(x)\,dx, \qquad r = 1, 2, \ldots. \tag{3.2}$$

Substituting the KMCG density in Eq (3.1) into Eq (3.2) gives

$$\mu'_r = \frac{\beta\pi\lambda}{2(e^{\beta}-1)} \int_0^{\infty} x^r e^{\alpha x} \exp\left[-\frac{\lambda}{\alpha}(e^{\alpha x}-1)\right] \times \sin\left[\frac{\pi}{2}\left\{1-\exp\left[-\frac{\lambda}{\alpha}(e^{\alpha x}-1)\right]\right\}\right] \times \exp\left\{\beta\left[1-\cos\left(\frac{\pi}{2}\left\{1-\exp\left[-\frac{\lambda}{\alpha}(e^{\alpha x}-1)\right]\right\}\right)\right]\right\} dx. \tag{3.3}$$

Since Eq (3.3) does not generally admit a simple closed-form expression, the moments are evaluated numerically. In particular, the first four raw moments are given by

$$\mu'_1 = E(X), \qquad \mu'_2 = E(X^2), \qquad \mu'_3 = E(X^3), \qquad \mu'_4 = E(X^4). \tag{3.4}$$

The mean and variance are

$$\mu = \mu'_1, \qquad \sigma^2 = \mu'_2 - (\mu'_1)^2. \tag{3.5}$$

The third and fourth central moments are

$$\mu_3 = \mu'_3 - 3\mu'_2\mu'_1 + 2(\mu'_1)^3, \tag{3.6}$$

$$\mu_4 = \mu'_4 - 4\mu'_3\mu'_1 + 6\mu'_2(\mu'_1)^2 - 3(\mu'_1)^4. \tag{3.7}$$

Accordingly, the skewness, kurtosis, and coefficient of variation are given by

$$\gamma_1 = \frac{\mu_3}{\sigma^3}, \qquad \gamma_2 = \frac{\mu_4}{\sigma^4}, \qquad CV = \frac{\sigma}{\mu'_1}. \tag{3.8}$$

These measures describe the location, dispersion, asymmetry, and shape characteristics of the KMCG distribution for different combinations of α, λ, and β.

Table 3 presents numerical values of the first four raw moments and related measures for selected parameter combinations, showing that the moments and shape measures vary substantially with the parameters; in particular, the KMCG distribution accommodates both positive and negative skewness, together with varying kurtosis and CV, demonstrating considerable flexibility in distributional shape.

Table 3. Moments and related measures of the KMCG distribution for selected parameter values.

α	λ	β	μ'_1	μ'_2	μ'_3	μ'_4	σ^2	Skewness	Kurtosis	CV
0.5	0.5	0.5	1.672741	3.438784	8.094961	21.053878	0.640721	0.388495	2.764557	0.478526
0.5	0.5	1.5	1.891864	4.221065	10.516727	28.479341	0.641914	0.198742	2.694972	0.423495
0.5	0.5	2.5	2.091515	4.981167	12.986005	36.333016	0.606732	0.063143	2.779012	0.372424
0.5	1.5	0.5	0.762731	0.779960	0.969249	1.390324	0.198201	0.815977	3.573499	0.583690
0.5	1.5	1.5	0.882802	0.990298	1.306365	1.948588	0.210959	0.615705	3.237969	0.520278
0.5	1.5	2.5	0.995054	1.201594	1.662796	2.560769	0.211461	0.476290	3.126820	0.462134
0.5	2.5	0.5	0.501858	0.350321	0.305574	0.314457	0.098460	1.001349	4.139535	0.625243
0.5	2.5	1.5	0.585595	0.450149	0.417160	0.446022	0.107227	0.796631	3.677592	0.559185
0.5	2.5	2.5	0.664637	0.551673	0.536701	0.592141	0.109930	0.656043	3.481234	0.498855
1.5	0.5	0.5	1.030364	1.209710	1.551167	2.125639	0.148060	-0.006801	2.600370	0.373447
1.5	0.5	1.5	1.135475	1.428923	1.929900	2.752175	0.139620	-0.185459	2.756965	0.329076
1.5	0.5	2.5	1.228853	1.634665	2.301120	3.388105	0.124586	-0.314659	3.026501	0.287233
1.5	1.5	0.5	0.557580	0.382087	0.299813	0.259924	0.071191	0.388495	2.764557	0.478526
1.5	1.5	1.5	0.630621	0.469007	0.389508	0.351597	0.071324	0.198742	2.694972	0.423495
1.5	1.5	2.5	0.697172	0.553463	0.480963	0.448556	0.067415	0.063143	2.779012	0.372424
1.5	2.5	0.5	0.395217	0.199907	0.118930	0.079702	0.043711	0.588001	3.059181	0.529003
1.5	2.5	1.5	0.452165	0.249550	0.157387	0.109770	0.045097	0.393290	2.869179	0.469655
1.5	2.5	2.5	0.504704	0.298579	0.197307	0.142152	0.043852	0.255688	2.861875	0.414916
2.5	0.5	0.5	0.779185	0.673337	0.625048	0.612931	0.066208	-0.163332	2.695943	0.330228
2.5	0.5	1.5	0.849103	0.781971	0.762490	0.777385	0.060995	-0.336336	2.938174	0.290862
2.5	0.5	2.5	0.910639	0.882519	0.894982	0.941316	0.053257	-0.461273	3.281785	0.253420
2.5	1.5	0.5	0.454529	0.244480	0.147011	0.096029	0.037883	0.196553	2.614629	0.428215
2.5	1.5	1.5	0.507866	0.294783	0.187230	0.127342	0.036856	0.011836	2.656556	0.378012
2.5	1.5	2.5	0.555864	0.342857	0.227482	0.159833	0.033872	-0.121218	2.829884	0.331093
2.5	2.5	0.5	0.334548	0.137551	0.064760	0.033686	0.025629	0.388495	2.764557	0.478526
2.5	2.5	1.5	0.378373	0.168843	0.084134	0.045567	0.025677	0.198742	2.694972	0.423495
2.5	2.5	2.5	0.418303	0.199247	0.103888	0.058133	0.024269	0.063143	2.779012	0.372424

3.2. Order statistics

Let

$$X_1, X_2, \ldots, X_n$$

be a random sample from the KMCG distribution with cumulative distribution function $F(x)$ and probability density function $f(x)$. Let

$$X_{1:n} \leq X_{2:n} \leq \cdots \leq X_{n:n}$$

denote the corresponding order statistics. The probability density function of the rth order statistic $X_{r:n}$ is given by

$$f_{r:n}(x) = \frac{n!}{(r-1)!(n-r)!}[F(x)]^{r-1}[1-F(x)]^{n-r}f(x), \qquad r = 1, 2, \ldots, n. \tag{3.9}$$

Using the survival function $S(x) = 1 - F(x)$, this expression may equivalently be written as

$$f_{r:n}(x) = \frac{n!}{(r-1)!(n-r)!}[F(x)]^{r-1}[S(x)]^{n-r}f(x). \tag{3.10}$$

For the KMCG distribution,

$$f_{r:n}(x) = \frac{n!}{(r-1)!(n-r)!}\left[\frac{e^{\beta R(x)}-1}{e^{\beta}-1}\right]^{r-1} \times \left[\frac{e^{\beta}-e^{\beta R(x)}}{e^{\beta}-1}\right]^{n-r}\frac{\beta r(x)e^{\beta R(x)}}{e^{\beta}-1}, \tag{3.11}$$

where $R(x)$ is defined in (2.7) and $r(x)$ is given in (2.11). The cumulative distribution function of the rth order statistic is

$$F_{r:n}(x) = \sum_{j=r}^{n}\binom{n}{j}[F(x)]^{j}[1-F(x)]^{n-j}. \tag{3.12}$$

Alternatively,

$$F_{r:n}(x) = \sum_{j=r}^{n}\binom{n}{j}[F(x)]^{j}[S(x)]^{n-j}. \tag{3.13}$$

Two important special cases are the sample minimum and sample maximum. For the minimum order statistic $X_{1:n}$,

$$F_{1:n}(x) = 1 - [1-F(x)]^{n} = 1 - [S(x)]^{n}, \tag{3.14}$$

and

$$f_{1:n}(x) = n[1-F(x)]^{n-1}f(x) = n[S(x)]^{n-1}f(x). \tag{3.15}$$

For the maximum order statistic $X_{n:n}$,

$$F_{n:n}(x) = [F(x)]^{n}, \tag{3.16}$$

and

$$f_{n:n}(x) = n[F(x)]^{n-1}f(x). \tag{3.17}$$

These order-statistic results are useful in reliability analysis, record-value problems, extreme-value investigations, and the study of sample minima and maxima from the KMCG distribution.

4. Parameter estimation

This section considers maximum likelihood and Bayesian estimation of the KMCG parameters. The estimation procedures and their numerical implementation are described in the following subsections.

4.1. Maximum likelihood estimation

Let

$$X_1, X_2, \ldots, X_n$$

be an independent random sample from the KMCG distribution with parameter vector

$$\boldsymbol{\theta} = (\alpha, \beta, \lambda)^{\top}, \qquad \alpha > 0, \quad \beta > 0, \quad \lambda > 0.$$

The likelihood function is defined by

$$L(\boldsymbol{\theta} \mid \mathbf{x}) = \prod_{i=1}^{n} f(x_i; \alpha, \beta, \lambda), \tag{4.1}$$

where $f(x; \alpha, \beta, \lambda)$ denotes the KMCG density given in Eq (2.17). For independent observations $x_1, \ldots, x_n > 0$, define

$$T_i = \frac{\lambda}{\alpha}\left(e^{\alpha x_i} - 1\right), \qquad s_i = e^{-T_i}, \qquad w_i = \frac{\pi}{2}(1 - s_i), \qquad H_i = 1 - \cos w_i.$$

Using these quantities, the log-likelihood can be written compactly as

$$\begin{aligned}\ell(\alpha, \beta, \lambda) = n \log\beta - n \log(e^{\beta} - 1) + n \log\left(\frac{\pi}{2}\right) + n \log\lambda + \alpha \sum_{i=1}^{n} x_i \\ - \sum_{i=1}^{n} T_i + \sum_{i=1}^{n} \log(\sin w_i) + \beta \sum_{i=1}^{n} H_i.\end{aligned} \tag{4.2}$$

Equivalently, before taking logarithms, the likelihood function is

$$\begin{aligned}L(\alpha, \beta, \lambda) = \left[\frac{\beta\pi\lambda}{2(e^{\beta} - 1)}\right]^n \exp\left(\alpha \sum_{i=1}^{n} x_i\right) \\ \times \exp\left(-\sum_{i=1}^{n} T_i\right) \prod_{i=1}^{n} \sin(w_i) \exp\left(\beta \sum_{i=1}^{n} H_i\right).\end{aligned} \tag{4.3}$$

The expression in Eq (4.2) contains all parameter-dependent terms and is therefore used for maximum likelihood estimation.

Score equations. For $\theta \in \{\alpha, \lambda\}$, define

$$D_i = \frac{\pi}{2} s_i \left(\cot w_i + \beta \sin w_i\right).$$

The required derivatives of T_i are

$$T_{i,\lambda} = \frac{e^{\alpha x_i} - 1}{\alpha}$$

and

$$T_{i,\alpha} = \frac{\lambda}{\alpha^2}\left[\alpha x_i e^{\alpha x_i} - (e^{\alpha x_i} - 1)\right].$$

The three score functions are therefore

$$U_{\alpha} = \frac{\partial \ell}{\partial \alpha} = \sum_{i=1}^{n} \left[x_i + (D_i - 1) T_{i,\alpha}\right], \tag{4.4}$$

$$U_{\beta} = \frac{\partial \ell}{\partial \beta} = \frac{n}{\beta} - \frac{n e^{\beta}}{e^{\beta} - 1} + \sum_{i=1}^{n} H_i, \tag{4.5}$$

$$U_\lambda = \frac{\partial \ell}{\partial \lambda} = \frac{n}{\lambda} + \sum_{i=1}^{n} (D_i - 1) T_{i,\lambda}. \tag{4.6}$$

The maximum likelihood estimates

$$\widehat{\alpha}, \qquad \widehat{\beta}, \qquad \widehat{\lambda}$$

are obtained by solving

$$U_\alpha = U_\beta = U_\lambda = 0,$$

subject to

$$\alpha > 0, \qquad \beta > 0, \qquad \lambda > 0.$$

Because the score equations are nonlinear and do not generally admit closed-form solutions, the MLEs are obtained numerically. The score vector is given by

$$U(\boldsymbol{\theta}) = \left(U_\alpha, U_\beta, U_\lambda\right)^\top. \tag{4.7}$$

The observed information matrix is defined by

$$J(\boldsymbol{\theta}) = -\frac{\partial^2 \ell(\boldsymbol{\theta})}{\partial \boldsymbol{\theta} \partial \boldsymbol{\theta}^\top}. \tag{4.8}$$

Under standard regularity conditions, the asymptotic distribution of the maximum likelihood estimator is

$$\widehat{\boldsymbol{\theta}} \tilde{\sim} N_3\left(\boldsymbol{\theta}, J^{-1}(\widehat{\boldsymbol{\theta}})\right). \tag{4.9}$$

Thus, an approximate $100(1-\gamma)\%$ confidence interval for a parameter θ_j is

$$\widehat{\theta}_j \pm z_{\gamma/2} \sqrt{\left[J^{-1}(\widehat{\boldsymbol{\theta}})\right]_{jj}}. \tag{4.10}$$

4.2. Bayesian estimation

In the Bayesian framework, the unknown KMCG parameters α, β, and λ are regarded as random variables. Since all model parameters are positive, independent Gamma prior distributions are considered. Specifically, let

$$\alpha \sim \text{Gamma}(a_\alpha, b_\alpha), \tag{4.11}$$

$$\beta \sim \text{Gamma}(a_\beta, b_\beta), \tag{4.12}$$

$$\lambda \sim \text{Gamma}(a_\lambda, b_\lambda), \tag{4.13}$$

where the Gamma distributions are parameterized in terms of shape and rate. Independent Gamma priors were adopted because the KMCG parameters α, β, and λ are strictly positive. The Gamma family provides support on $(0, \infty)$ and permits direct control of the prior location and dispersion. However, we emphasize that parameter-dependent Gamma specifications should not automatically be interpreted as non-informative priors, particularly when the likelihood is weakly informative or the posterior is concentrated near the boundary of the parameter space.

For this reason, the posterior results are interpreted jointly with prior-sensitivity results and likelihood-based estimates. Particular caution is exercised for parameters whose maximum likelihood or posterior estimates are close to zero, since in such cases the prior may provide non-negligible regularization. Thus, agreement between the Bayesian and maximum likelihood estimates is considered supportive evidence, whereas noticeable prior sensitivity is explicitly reported rather than interpreted as information supplied solely by the data. Accordingly, the prior density of α is

$$\pi(\alpha) = \frac{b_\alpha^{a_\alpha}}{\Gamma(a_\alpha)} \alpha^{a_\alpha - 1} e^{-b_\alpha \alpha}, \qquad \alpha > 0. \tag{4.14}$$

Similarly,

$$\pi(\beta) = \frac{b_\beta^{a_\beta}}{\Gamma(a_\beta)} \beta^{a_\beta - 1} e^{-b_\beta \beta}, \qquad \beta > 0, \tag{4.15}$$

and

$$\pi(\lambda) = \frac{b_\lambda^{a_\lambda}}{\Gamma(a_\lambda)} \lambda^{a_\lambda - 1} e^{-b_\lambda \lambda}, \qquad \lambda > 0. \tag{4.16}$$

Assuming prior independence, the joint prior density is

$$\pi(\alpha, \beta, \lambda) = \pi(\alpha)\pi(\beta)\pi(\lambda). \tag{4.17}$$

By Bayes' theorem, the joint posterior density is proportional to the product of the likelihood and the joint prior:

$$\pi(\alpha, \beta, \lambda \mid \mathbf{x}) \propto L(\alpha, \beta, \lambda \mid \mathbf{x})\pi(\alpha, \beta, \lambda). \tag{4.18}$$

Consequently,

$$\begin{aligned} \pi(\alpha, \beta, \lambda \mid \mathbf{x}) \propto\ & L(\alpha, \beta, \lambda \mid \mathbf{x}) \alpha^{a_\alpha - 1} e^{-b_\alpha \alpha} \\ & \times \beta^{a_\beta - 1} e^{-b_\beta \beta} \lambda^{a_\lambda - 1} e^{-b_\lambda \lambda}. \end{aligned} \tag{4.19}$$

The normalized posterior density can be expressed as

$$\pi(\boldsymbol{\theta} \mid \mathbf{x}) = \frac{L(\boldsymbol{\theta} \mid \mathbf{x})\pi(\boldsymbol{\theta})}{\displaystyle\int_0^\infty \int_0^\infty \int_0^\infty L(\boldsymbol{\theta} \mid \mathbf{x})\pi(\boldsymbol{\theta})\, d\alpha\, d\beta\, d\lambda}. \tag{4.20}$$

Under squared-error loss, the Bayesian estimator of a parameter is its posterior mean. Therefore,

$$\widehat{\alpha}_B = E(\alpha \mid \mathbf{x}), \tag{4.21}$$

$$\widehat{\beta}_B = E(\beta \mid \mathbf{x}), \tag{4.22}$$

$$\widehat{\lambda}_B = E(\lambda \mid \mathbf{x}). \tag{4.23}$$

Posterior sampling was performed using a random-walk Metropolis–Hastings algorithm. Since the KMCG parameters are positive, the algorithm was implemented on the logarithmic parameter scale,

$$\boldsymbol{\eta} = (\log \alpha, \log \beta, \log \lambda)^\top.$$

At iteration m, the candidate vector was generated from

$$\boldsymbol{\eta}^{*} = \boldsymbol{\eta}^{(m-1)} + \boldsymbol{\varepsilon}, \qquad \boldsymbol{\varepsilon} \sim N_3(\mathbf{0}, \boldsymbol{\Sigma}_q),$$

where $\boldsymbol{\Sigma}_q$ denotes the proposal covariance matrix.

The proposal variances were tuned during preliminary runs to obtain stable mixing and a reasonable acceptance rate. After tuning, the proposal variances were fixed during the retained sampling stage. The final proposal standard deviations used for each parameter were reported together with the corresponding MCMC settings to ensure reproducibility. In general, these posterior expectations do not possess convenient closed-form expressions. Therefore, posterior inference is performed using Markov chain Monte Carlo (MCMC) simulation. A random-walk Metropolis–Hastings procedure may be employed to generate draws

$$\boldsymbol{\theta}^{(1)}, \boldsymbol{\theta}^{(2)}, \ldots, \boldsymbol{\theta}^{(M)}$$

from the posterior distribution. After discarding the burn-in iterations, the Bayesian estimates can be approximated by

$$\widehat{\theta}_B = \frac{1}{M} \sum_{m=1}^{M} \theta^{(m)}. \tag{4.24}$$

A proposed value $\boldsymbol{\theta}^{*}$ is accepted with probability

$$A = \min\left\{1, \frac{\pi(\boldsymbol{\theta}^{*} \mid \mathbf{x}) q(\boldsymbol{\theta}^{(m-1)} \mid \boldsymbol{\theta}^{*})}{\pi(\boldsymbol{\theta}^{(m-1)} \mid \mathbf{x}) q(\boldsymbol{\theta}^{*} \mid \boldsymbol{\theta}^{(m-1)})}\right\}, \tag{4.25}$$

where $q(\cdot \mid \cdot)$ denotes the proposal density. For a symmetric random-walk proposal distribution,

$$q(\boldsymbol{\theta}^{(m-1)} \mid \boldsymbol{\theta}^{*}) = q(\boldsymbol{\theta}^{*} \mid \boldsymbol{\theta}^{(m-1)}), \tag{4.26}$$

and hence the acceptance probability reduces to

$$A = \min\left\{1, \frac{\pi(\boldsymbol{\theta}^{*} \mid \mathbf{x})}{\pi(\boldsymbol{\theta}^{(m-1)} \mid \mathbf{x})}\right\}. \tag{4.27}$$

Posterior uncertainty is summarized by equal-tail and highest posterior density (HPD) credible intervals. A $100(1-\gamma)\%$ equal-tail credible interval for a parameter θ is

$$\left[Q_{\theta|\mathbf{x}}\left(\frac{\gamma}{2}\right), Q_{\theta|\mathbf{x}}\left(1-\frac{\gamma}{2}\right)\right], \tag{4.28}$$

where $Q_{\theta|\mathbf{x}}(\cdot)$ denotes the posterior quantile function. The HPD interval is the shortest posterior interval $C_{1-\gamma}$ satisfying

$$P\left(\theta \in C_{1-\gamma} \mid \mathbf{x}\right) = 1-\gamma. \tag{4.29}$$

The convergence and efficiency of the MCMC procedure are assessed using acceptance rates, effective sample sizes (ESS), Monte Carlo standard errors (MCSE), MCSE-to-posterior-standard-deviation ratios, and Gelman–Rubin $\widehat{R}$ statistics.

5. Simulation study

A Monte Carlo simulation study was conducted to investigate the finite-sample performance of the maximum likelihood (ML) and Bayesian estimators of the CMG distribution. Two parameter settings were considered. The first simulation setting was defined by

$$(\alpha, \beta, \lambda) = (1.2, 1.5, 0.8),$$

whereas the second simulation setting was defined by

$$(\alpha, \beta, \lambda) = (1.5, 1.2, 1.1).$$

For each parameter setting, samples of sizes

$$n = 50, 150, 250, 350, \text{ and } 400$$

were considered. Let $\boldsymbol{\eta} = (\alpha, \beta, \lambda)^{\mathsf{T}}$ and $\widehat{\eta}_{j,r}$ denote the estimate of η_j in the rth Monte Carlo replication. The mean estimate, bias, relative bias (RB), MSE, and RMSE were calculated as

$$\overline{\widehat{\eta}}_j = \frac{1}{N_{\mathrm{MC}}} \sum_{r=1}^{N_{\mathrm{MC}}} \widehat{\eta}_{j,r}, \qquad \mathrm{Bias}_j = \overline{\widehat{\eta}}_j - \eta_{j,0},$$

$$\mathrm{RB}_j = \frac{\mathrm{Bias}_j}{\eta_{j,0}}, \qquad \mathrm{MSE}_j = \frac{1}{N_{\mathrm{MC}}} \sum_{r=1}^{N_{\mathrm{MC}}} (\widehat{\eta}_{j,r} - \eta_{j,0})^2, \qquad \mathrm{RMSE}_j = \sqrt{\mathrm{MSE}_j}.$$

For ML estimation,

$$\widehat{\boldsymbol{\eta}}_{\mathrm{ML}} = \arg\max_{\boldsymbol{\eta}} \ell(\boldsymbol{\eta}; \boldsymbol{x}), \qquad \ell(\boldsymbol{\eta}; \boldsymbol{x}) = \sum_{i=1}^{n} \log f(x_i; \boldsymbol{\eta}).$$

Standard errors were obtained from the inverse observed information matrix, and nominal 95% Wald confidence intervals were calculated as

$$\widehat{\eta}_j \pm 1.96 \ \mathrm{SE}(\widehat{\eta}_j).$$

Coverage and average interval length were recorded together with the convergence, positive-Hessian, reliable-CI, and boundary rates. For Bayesian estimation,

$$\pi(\boldsymbol{\eta} \mid \boldsymbol{x}) \propto L(\boldsymbol{\eta}; \boldsymbol{x}) \pi(\boldsymbol{\eta}), \qquad L(\boldsymbol{\eta}; \boldsymbol{x}) = \prod_{i=1}^{n} f(x_i; \boldsymbol{\eta}),$$

and the posterior mean was used as the point estimator. The bias, RB, MSE, and RMSE were calculated as above. Equal-tail and HPD 95% credible intervals were also evaluated. MCMC performance was assessed using the acceptance rate (AR), effective sample size (ESS), Monte Carlo standard error (MCSE), and Gelman–Rubin statistic $\widehat{R}$. Prior sensitivity was examined using independent Gamma priors,

$$\eta_j \sim \mathrm{Gamma}(a_j, b_j),$$

with

$$\mathrm{Gamma}(2, 1), \qquad \mathrm{Gamma}(1, 0.5), \qquad \mathrm{Gamma}(0.5, 0.1).$$

5.1. First simulation setting

For the first parameter setting, the true parameter vector was taken as

$$(\alpha, \beta, \lambda) = (1.2, 1.5, 0.8).$$

The finite-sample performance of the maximum likelihood (ML) and Bayesian estimators was investigated for sample sizes $n = 50, 150, 250, 350$, and 400.

Table 4 presents the maximum likelihood estimation results. For α, the mean estimates remain close to the true value across the considered sample sizes, with biases ranging from approximately -0.002 to 0.039. The RMSE decreases overall from 0.4676 at $n = 50$ to 0.2575 at $n = 400$, although a small non-monotone fluctuation is observed at the intermediate sample sizes. For β, the largest estimation variability is observed at the smallest sample size, with an RMSE of 2.3180 at $n = 50$. The RMSE decreases substantially with increasing sample size and reaches 1.0614 at $n = 400$. The estimates of λ also become progressively more stable, with the RMSE decreasing from 0.6302 at $n = 50$ to 0.2886 at $n = 400$. Thus, increasing the sample size generally improves estimation precision for all three parameters, while β remains the most variable parameter.

Table 4. Maximum likelihood estimation performance for $(\alpha, \beta, \lambda) = (1.2, 1.5, 0.8)$.

n	Parameter	True value	Mean estimate	Bias	Relative bias	MSE	RMSE
50	α	1.2	1.197682	-0.002318	-0.001931	0.218634	0.467583
	β	1.5	1.942857	0.442857	0.295238	5.372998	2.317973
	λ	0.8	0.950845	0.150845	0.188557	0.397155	0.630202
150	α	1.2	1.216969	0.016969	0.014140	0.103773	0.322138
	β	1.5	1.538066	0.038066	0.025378	1.821175	1.349509
	λ	0.8	0.842307	0.042307	0.052884	0.150283	0.387663
250	α	1.2	1.238915	0.038915	0.032429	0.081214	0.284980
	β	1.5	1.392924	-0.107076	-0.071384	1.393511	1.180471
	λ	0.8	0.800834	0.000834	0.001043	0.104323	0.322990
350	α	1.2	1.236305	0.036305	0.030254	0.066732	0.258325
	β	1.5	1.375438	-0.124562	-0.083041	1.168377	1.080915
	λ	0.8	0.796261	-0.003739	-0.004674	0.086319	0.293801
400	α	1.2	1.233613	0.033613	0.028011	0.066282	0.257453
	β	1.5	1.387758	-0.112242	-0.074828	1.126501	1.061368
	λ	0.8	0.798362	-0.001638	-0.002048	0.083268	0.288563

Table 5 summarizes the numerical diagnostics associated with the maximum likelihood estimation. The convergence rates are very high, ranging from 0.997 to 1.000, and the positive Hessian rates are between 0.998 and 1.000. The rate of reliable confidence intervals increases from 0.531 at $n = 50$ to 0.705 at $n = 400$, indicating improved numerical reliability as the sample size increases. The median Hessian condition numbers range from 961.5321 to 1613.1336, indicating that the numerical conditioning of the observed information matrix should still be taken into account when constructing likelihood-based intervals. The boundary rate for α is negligible, ranging from 0.003 at $n = 50$ to zero for the larger sample sizes. The boundary rate for λ is zero for all sample sizes. In contrast, the boundary rate for β remains non-negligible, decreasing from 0.180 at $n = 50$ to 0.121 at $n = 400$. This behavior is consistent with the comparatively greater estimation variability observed for β.

Table 5. Numerical diagnostics for maximum likelihood estimation.

n	Convergence rate	Positive hessian rate	Reliable CI rate	Median hessian condition	Boundary rate α	Boundary rate β	Boundary rate λ
50	1.000	0.998	0.531	961.5321	0.003	0.180	0.000
150	0.999	0.998	0.638	1202.1670	0.000	0.155	0.000
250	0.999	0.999	0.667	1504.8941	0.000	0.145	0.000
350	1.000	1.000	0.702	1613.1336	0.000	0.141	0.000
400	0.997	0.997	0.705	1516.9844	0.000	0.121	0.000

The performance of the nominal 95% Wald confidence intervals is summarized in Table 6. The coverage probabilities for α remain close to the nominal level, ranging from 0.955 to 0.994. In contrast, the coverage probabilities for β are consistently below the nominal level, ranging from 0.733 to 0.845, indicating that the Wald approximation is less reliable for this parameter. The coverage probabilities for λ range from 0.825 to 0.893, and therefore also remain below the nominal level. The mean interval lengths generally decrease as the sample size increases, reflecting increasing precision with larger samples.

Table 6. Performance of nominal 95% Wald confidence intervals.

n	Parameter	Coverage	MCSE of coverage	Valid CI count	Mean lower	Mean upper	Mean length
50	α	0.994350	0.003253	531	0.334816	2.659169	2.202967
	β	0.732580	0.019208	531	0.630052	14.083353	13.002793
	λ	0.824859	0.016494	531	0.362209	3.625843	3.071823
150	α	0.981191	0.005378	638	0.558911	1.970904	1.306998
	β	0.794671	0.015992	638	0.559486	8.060573	7.020796
	λ	0.849530	0.014155	638	0.396592	2.347405	1.777845
250	α	0.970015	0.006604	667	0.660114	1.848658	1.067805
	β	0.814093	0.015063	667	0.497281	6.599165	5.681904
	λ	0.875562	0.012781	667	0.410465	1.957290	1.377045
350	α	0.961538	0.007258	702	0.697433	1.767863	0.977128
	β	0.844729	0.013669	702	0.536108	5.857997	4.992961
	λ	0.893162	0.011659	702	0.438311	1.841255	1.229454
400	α	0.954610	0.007840	705	0.706195	1.699841	0.906227
	β	0.819858	0.014474	705	0.634863	5.412072	4.462798
	λ	0.879433	0.012264	705	0.472269	1.750046	1.148687

The Bayesian estimation results are reported in Table 7. The posterior means of α are below its true value for all sample sizes, with the absolute bias decreasing from 0.1162 at $n = 50$ to 0.0360 at $n = 400$. In contrast, the posterior mean of β is consistently above its true value, although the bias decreases from 0.5164 to 0.1571 as the sample size increases. Similarly, the posterior mean of λ exceeds the true value, with the bias decreasing from 0.2001 at $n = 50$ to 0.0658 at $n = 400$. The MSE and RMSE values decrease systematically with increasing sample size.

Table 8 gives the coverage probabilities of the nominal 95% Bayesian credible intervals. For α, equal-tail coverage ranges from 0.938 to 0.964, whereas HPD coverage ranges from 0.923 to 0.952. For β, equal-tail coverage ranges from 0.935 to 0.980, while HPD coverage ranges from 0.926 to 0.983. For λ, the corresponding ranges are 0.935–0.979 for equal-tail intervals and 0.929–0.980 for HPD intervals. The MCSE values are generally small, indicating adequate Monte Carlo precision.

Table 7. Bayesian estimation performance for $(\alpha, \beta, \lambda) = (1.2, 1.5, 0.8)$.

n	Parameter	True value	Mean estimate	Bias	Relative bias	MSE	RMSE
50	α	1.2	1.083756	-0.116244	-0.096870	0.068173	0.261099
	β	1.5	2.016391	0.516391	0.344261	0.697472	0.835148
	λ	0.8	1.000060	0.200060	0.250076	0.085740	0.292813
150	α	1.2	1.121732	-0.078268	-0.065223	0.037434	0.193478
	β	1.5	1.844311	0.344311	0.229541	0.504116	0.710011
	λ	0.8	0.927691	0.127691	0.159613	0.054553	0.233567
250	α	1.2	1.143854	-0.056146	-0.046788	0.030284	0.174023
	β	1.5	1.742349	0.242349	0.161566	0.439136	0.662673
	λ	0.8	0.894549	0.094549	0.118187	0.043048	0.207480
350	α	1.2	1.154265	-0.045735	-0.038112	0.025699	0.160309
	β	1.5	1.694941	0.194941	0.129961	0.371770	0.609730
	λ	0.8	0.878696	0.078696	0.098370	0.035982	0.189688
400	α	1.2	1.164000	-0.036000	-0.030000	0.024139	0.155366
	β	1.5	1.657073	0.157073	0.104716	0.346189	0.588379
	λ	0.8	0.865810	0.065810	0.082262	0.033128	0.182011

Table 8. Coverage of nominal 95% Bayesian credible intervals.

n	Parameter	Equal-tail coverage	HPD coverage	MCSE equal-tail	MCSE HPD
50	α	0.963	0.947	0.005969	0.007085
	β	0.980	0.983	0.004427	0.004088
	λ	0.979	0.980	0.004534	0.004427
150	α	0.964	0.952	0.005891	0.006760
	β	0.961	0.966	0.006122	0.005731
	λ	0.965	0.966	0.005812	0.005731
250	α	0.950	0.933	0.006892	0.007906
	β	0.945	0.931	0.007209	0.008015
	λ	0.944	0.946	0.007271	0.007147
350	α	0.942	0.937	0.007392	0.007683
	β	0.934	0.927	0.007851	0.008226
	λ	0.935	0.936	0.007796	0.007740
400	α	0.938	0.923	0.007626	0.008430
	β	0.935	0.926	0.007796	0.008278
	λ	0.935	0.929	0.007796	0.008122

The Bayesian interval endpoints and lengths are presented in Table 9. Both equal-tail and HPD intervals become shorter as the sample size increases. The HPD intervals are generally slightly shorter than the corresponding equal-tail intervals.

The average MCMC acceptance rates and the number of successful fits are reported in Table 10. The acceptance rate decreases from 0.4854 at $n = 50$ to 0.1722 at $n = 400$. Despite this decline, all 1000 Bayesian fits were successful at every sample size, and all resulting equal-tail and HPD intervals were valid.

For the illustrative sample, the detailed MCMC diagnostics are given in Table 11. The effective sample sizes are all above 2250, and the MCSE-to-SD ratios are small. The reported $\widehat{R}$ values are extremely close to one. The corresponding upper confidence limits are reported separately in Table 12.

Table 9. Bayesian credible interval endpoints and lengths.

n	Parameter	Equal-tail lower	Equal-tail upper	Equal-tail length	HPD lower	HPD upper	HPD length
50	α	0.525021	1.668397	1.143376	0.517331	1.634722	1.117390
	β	0.567791	4.265715	3.697924	0.469240	3.917814	3.448574
	λ	0.508312	1.732171	1.223859	0.472821	1.643018	1.170197
150	α	0.691156	1.531390	0.840233	0.700059	1.519416	0.819358
	β	0.619449	3.566097	2.946648	0.559173	3.339078	2.779905
	λ	0.551163	1.484083	0.932919	0.527986	1.416091	0.888105
250	α	0.768023	1.490180	0.722157	0.782697	1.483435	0.700738
	β	0.656868	3.230153	2.573285	0.610458	3.043156	2.432698
	λ	0.568926	1.370150	0.801224	0.552388	1.312863	0.760475
350	α	0.818725	1.464923	0.646198	0.833196	1.459210	0.626014
	β	0.685344	3.030942	2.345598	0.648315	2.868211	2.219896
	λ	0.582962	1.298364	0.715402	0.568914	1.247942	0.679028
400	α	0.838782	1.457442	0.618660	0.854065	1.453150	0.599085
	β	0.694227	2.937036	2.242809	0.663067	2.791736	2.128669
	λ	0.585445	1.268232	0.682787	0.573673	1.223402	0.649730

Table 10. Average MCMC acceptance rates and successful fits in the simulation.

n	Acceptance rate	Successful fits	Valid equal-tail intervals	Valid HPD intervals
50	0.485392	1000	1000	1000
150	0.304292	1000	1000	1000
250	0.230973	1000	1000	1000
350	0.187964	1000	1000	1000
400	0.172205	1000	1000	1000

Table 11. MCMC diagnostics for the illustrative sample.

Parameter	Posterior mean	Posterior SD	ESS	MCSE	MCSE/SD	Acceptance rate	$\widehat{R}$
α	1.241715	0.193383	3179.865	0.003429	0.017734	0.254967	1.000230
β	1.689923	0.719494	2250.445	0.015167	0.021080	0.254967	1.000255
λ	0.825696	0.204003	3193.848	0.003610	0.017695	0.254967	1.000191

Table 12. Upper confidence limits for the Gelman–Rubin diagnostic.

Parameter	$\widehat{R}$	Upper confidence limit
α	1.000230	1.000482
β	1.000255	1.000670
λ	1.000191	1.000345

The prior sensitivity analysis is summarized in Table 13. Three Gamma priors were considered. The posterior summaries for α, β, and λ remain broadly comparable across the three prior specifications, although some prior sensitivity is visible, particularly for β.

Table 13. Prior sensitivity analysis for the illustrative sample.

Prior	Parameter	Posterior mean	Posterior SD	HPD lower	HPD upper	Acceptance rate
Gamma(2, 1)	α	1.240826	0.192823	0.854413	1.606327	0.257033
	β	1.681993	0.740870	0.110592	2.943862	0.257033
	λ	0.825752	0.206583	0.448744	1.229583	0.257033
Gamma(1, 0.5)	α	1.277963	0.204761	0.894444	1.670680	0.253600
	β	1.537494	0.772142	0.114320	2.863660	0.253600
	λ	0.786944	0.213210	0.428752	1.190226	0.253600
Gamma(0.5, 0.1)	α	1.287537	0.220219	0.852962	1.673480	0.264400
	β	1.499078	0.839491	0.028219	2.923298	0.264400
	λ	0.778653	0.229337	0.411785	1.216544	0.264400

Figure 5 illustrates the probability density function, cumulative distribution function, and hazard function associated with the first parameter setting. Figure 6 compares the MSE values of the maximum likelihood and Bayesian estimators for α, β, and λ. For all three parameters, the MSE decreases as the sample size increases, indicating improved estimation precision. The Bayesian MSE values are smaller than the corresponding MLE MSE values throughout the displayed sample-size range. Figure 7 presents the MCMC trace plots and posterior distributions obtained for the three model parameters under the first simulation setting. The trace plots exhibit stable sampling behavior without pronounced systematic trends over the iterations. The posterior distribution of β is more dispersed than those of α and λ, which is consistent with the larger posterior standard deviation and wider credible intervals reported in Tables 9 and 11. The Wald confidence intervals obtained from maximum likelihood estimation are generally wider than the Bayesian credible intervals, particularly for β. The Bayesian equal-tail and HPD intervals become progressively shorter as the sample size increases. Overall, the simulation results indicate that increasing the sample size generally improves the numerical precision of both estimation procedures.

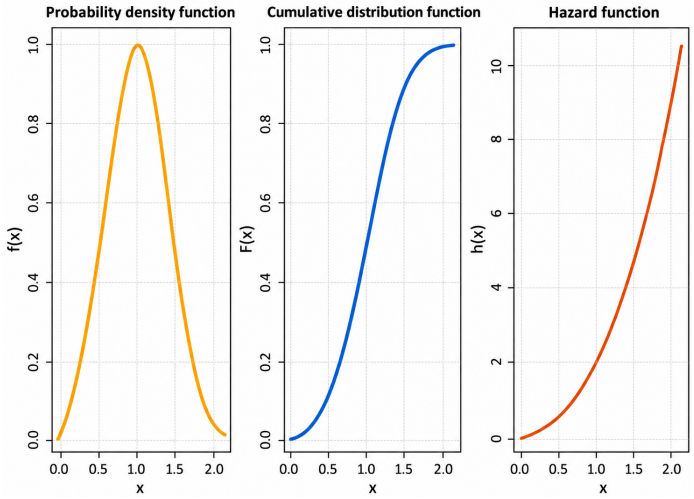


Figure 5. Probability density function, cumulative distribution function, and hazard function of the model under the first parameter setting, $(\alpha, \beta, \lambda) = (1.2, 1.5, 0.8)$.

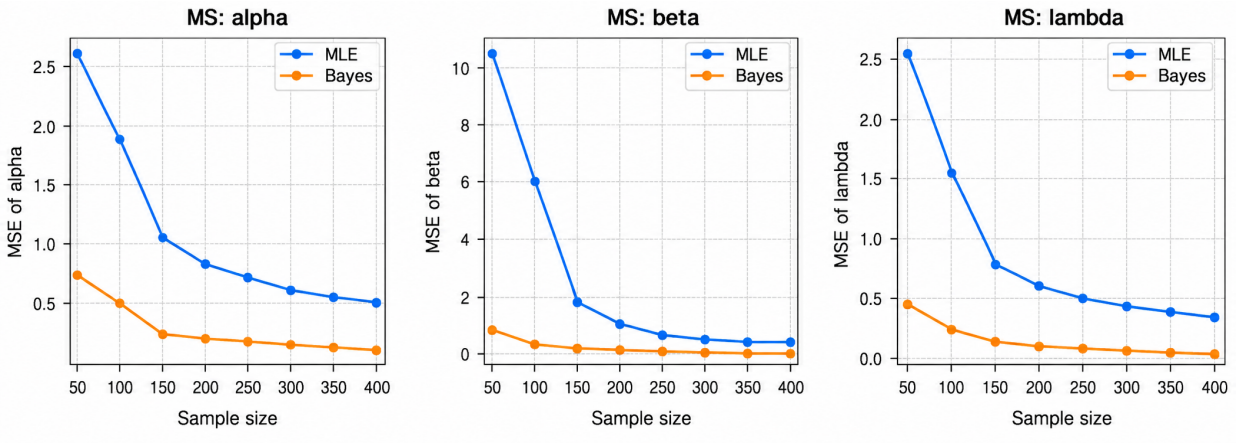


Figure 6. Comparison of the mean squared errors (MSEs) of the maximum likelihood and Bayesian estimators for α, β, and λ at different sample sizes under the first simulation setting, $(\alpha, \beta, \lambda) = (1.2, 1.5, 0.8)$.

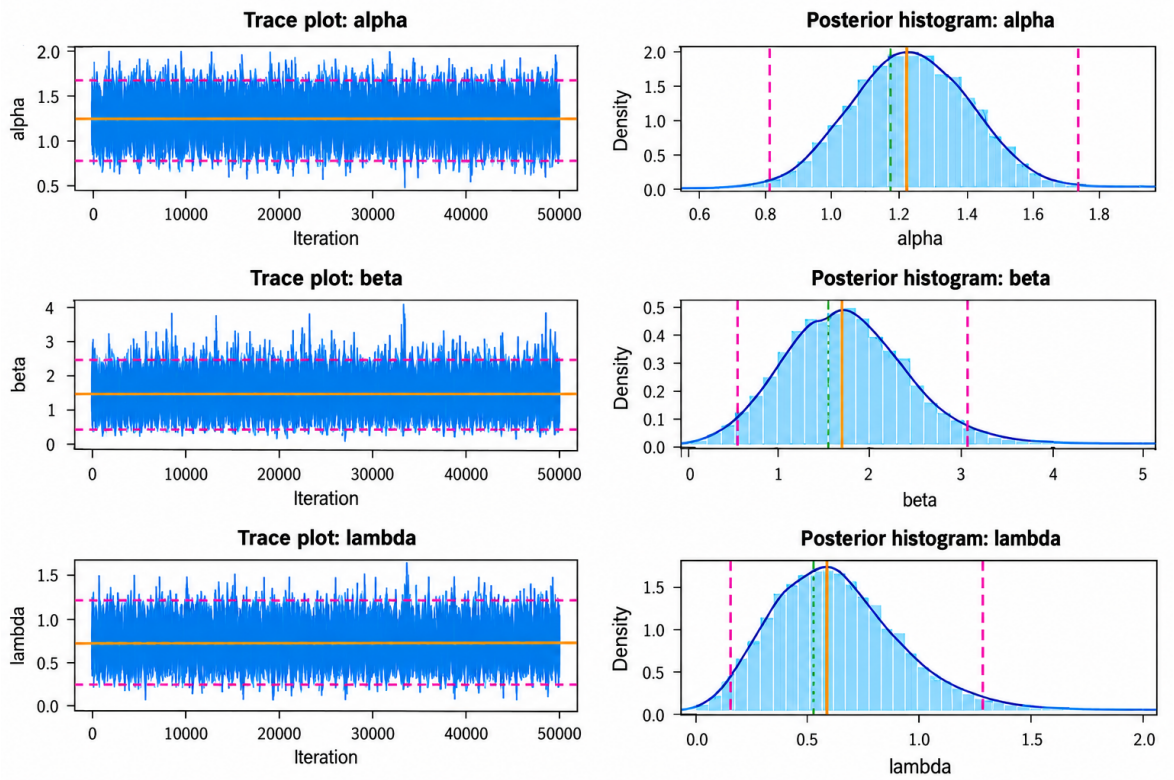


Figure 7. MCMC trace plots and posterior distributions for α, β, and λ under the first simulation setting, with $(\alpha, \beta, \lambda) = (1.2, 1.5, 0.8)$.

5.2. *Second simulation setting*

For the second parameter setting, the true parameter vector was taken as

$$(\alpha, \beta, \lambda) = (1.5, 1.2, 1.1).$$

The finite-sample performance of the maximum likelihood (ML) and Bayesian estimators was investigated for sample sizes $n = 50, 150, 250, 350$, and 400.

Table 14 summarizes the ML results. For α, the mean estimates remain close to the true value, with RMSE decreasing from 0.5860 at $n = 50$ to 0.3141 at $n = 400$. For β, the RMSE decreases from 2.0846 to 0.9886, while for λ it decreases from 0.8286 to 0.3929. Thus, increasing the sample size generally improves estimation precision, although β remains relatively variable.

Table 15 shows that the ML convergence and positive Hessian rates are close to one for all sample sizes. The reliable CI rate increases from 0.447 to 0.660. The boundary rate for β is noticeable but decreases from 0.237 to 0.160, whereas the boundary rates for α and λ are negligible.

Table 14. Maximum likelihood estimation performance for $(\alpha, \beta, \lambda) = (1.5, 1.2, 1.1)$ under the second simulation setting.

n	Parameter	True value	Mean estimate	Bias	Relative bias	MSE	RMSE
50	α	1.5	1.492047	-0.007953	-0.005302	0.343393	0.585997
	β	1.2	1.603515	0.403515	0.336263	4.345656	2.084624
	λ	1.1	1.297396	0.197396	0.179451	0.686648	0.828642
150	α	1.5	1.486376	-0.013624	-0.009083	0.158071	0.397582
	β	1.2	1.336918	0.136918	0.114098	1.645828	1.282898
	λ	1.1	1.194082	0.094082	0.085529	0.282587	0.531589
250	α	1.5	1.516023	0.016023	0.010682	0.119685	0.345955
	β	1.2	1.193910	-0.006090	-0.005075	1.209383	1.099719
	λ	1.1	1.135082	0.035082	0.031893	0.187876	0.433447
350	α	1.5	1.517620	0.017620	0.011747	0.099571	0.315549
	β	1.2	1.160538	-0.039462	-0.032885	1.025446	1.012643
	λ	1.1	1.124537	0.024537	0.022306	0.160114	0.400143
400	α	1.5	1.508290	0.008290	0.005527	0.098684	0.314140
	β	1.2	1.193185	-0.006815	-0.005679	0.977379	0.988625
	λ	1.1	1.134851	0.034851	0.031683	0.154332	0.392852

Table 15. Numerical diagnostics for maximum likelihood estimation under the second simulation setting.

n	Convergence rate	Positive hessian rate	Reliable CI rate	Median hessian condition	Boundary rate α	Boundary rate β	Boundary rate λ
50	0.997	0.997	0.447	1291.990	0.005	0.237	0.000
150	0.999	0.995	0.573	1487.026	0.000	0.194	0.000
250	0.997	0.995	0.615	1810.573	0.000	0.193	0.000
350	0.997	0.995	0.633	2081.850	0.000	0.193	0.000
400	0.994	0.997	0.660	1880.502	0.000	0.160	0.000

The nominal 95% Wald interval results are given in Table 16. Coverage for α is close to the nominal level, whereas coverage for β and λ is generally lower. The mean interval lengths decrease with increasing sample size.

The Bayesian estimation results in Table 17 show decreasing MSE and RMSE as the sample size increases. The posterior means of α are below the true value, whereas those of β and λ are above their true values. The corresponding biases decrease in magnitude as n increases.

Table 16. Performance of nominal 95% Wald confidence intervals under the second simulation setting.

n	Parameter	Coverage	MCSE of coverage	Valid CI count	Mean lower	Mean upper	Mean length
50	α	0.995526	0.003157	447	0.376069	3.496707	2.952697
	β	0.713647	0.021382	447	0.524867	13.439810	12.337074
	λ	0.825503	0.017951	447	0.527092	5.065459	4.167685
150	α	0.993019	0.003478	573	0.631476	2.467927	1.709511
	β	0.759162	0.017863	573	0.522321	7.984366	7.077008
	λ	0.821990	0.015980	573	0.596218	3.340058	2.509535
250	α	0.972358	0.006611	615	0.768381	2.297507	1.380154
	β	0.770732	0.016951	615	0.394102	6.557068	5.936930
	λ	0.860163	0.013985	615	0.595752	2.770771	1.940402
350	α	0.962085	0.007591	633	0.812496	2.210718	1.261173
	β	0.802528	0.015823	633	0.424310	5.809778	5.080864
	λ	0.864139	0.013619	633	0.629296	2.613853	1.738443
400	α	0.954545	0.008108	660	0.828003	2.124006	1.180945
	β	0.777273	0.016196	660	0.458837	5.398047	4.688015
	λ	0.850000	0.013899	660	0.669701	2.503965	1.627164

Table 17. Bayesian estimation performance for $(\alpha, \beta, \lambda) = (1.5, 1.2, 1.1)$ under the second simulation setting.

n	Parameter	True value	Mean estimate	Bias	Relative bias	MSE	RMSE
50	α	1.5	1.315962	-0.184038	-0.122692	0.119601	0.345833
	β	1.2	1.832798	0.632798	0.527332	0.732194	0.855684
	λ	1.1	1.414019	0.314019	0.285471	0.173077	0.416025
150	α	1.5	1.354529	-0.145471	-0.096980	0.070117	0.264797
	β	1.2	1.679830	0.479830	0.399858	0.536134	0.732212
	λ	1.1	1.328805	0.228805	0.208004	0.117107	0.342208
250	α	1.5	1.389061	-0.110939	-0.073960	0.052796	0.229774
	β	1.2	1.560922	0.360922	0.300769	0.431462	0.656858
	λ	1.1	1.274882	0.174882	0.158984	0.087435	0.295694
350	α	1.5	1.399789	-0.100211	-0.066808	0.045461	0.213216
	β	1.2	1.523660	0.323660	0.269717	0.386729	0.621875
	λ	1.1	1.257903	0.157903	0.143548	0.077482	0.278356
400	α	1.5	1.403938	-0.096062	-0.064041	0.044867	0.211819
	β	1.2	1.512348	0.312348	0.260290	0.371705	0.609676
	λ	1.1	1.251046	0.151046	0.137315	0.075000	0.273861

Table 18 presents the coverage of the nominal 95% Bayesian credible intervals. Equal-tail and HPD coverages are generally close to the nominal level for smaller and moderate sample sizes, although some reduction is observed at larger sample sizes. Table 19 shows that both types of credible intervals become shorter as the sample size increases.

Table 18. Coverage of nominal 95% Bayesian credible intervals under the second simulation setting.

n	Parameter	Equal-tail coverage	HPD coverage	MCSE equal-tail	MCSE HPD
50	α	0.942	0.922	0.007392	0.008480
	β	0.976	0.986	0.004840	0.003715
	λ	0.967	0.975	0.005649	0.004937
150	α	0.953	0.935	0.006693	0.007796
	β	0.957	0.968	0.006415	0.005566
	λ	0.954	0.965	0.006624	0.005812
250	α	0.953	0.935	0.006693	0.007796
	β	0.941	0.940	0.007451	0.007510
	λ	0.943	0.944	0.007332	0.007271
350	α	0.931	0.918	0.008015	0.008676
	β	0.918	0.916	0.008676	0.008772
	λ	0.925	0.924	0.008329	0.008380
400	α	0.925	0.915	0.008329	0.008819
	β	0.916	0.911	0.008772	0.009004
	λ	0.921	0.919	0.008530	0.008628

Table 19. Bayesian credible interval endpoints and lengths under the second simulation setting.

n	Parameter	Equal-tail lower	Equal-tail upper	Equal-tail length	HPD lower	HPD upper	HPD length
50	α	0.610406	2.056912	1.446506	0.598207	2.011341	1.413134
	β	0.490870	3.956148	3.465278	0.396433	3.617270	3.220837
	λ	0.752303	2.390016	1.637712	0.705060	2.274700	1.569640
150	α	0.806402	1.873970	1.067568	0.817390	1.860320	1.042931
	β	0.534090	3.320224	2.786134	0.475580	3.098229	2.622649
	λ	0.813064	2.084692	1.271628	0.781315	1.995969	1.214654
250	α	0.916983	1.822400	0.905417	0.932416	1.813740	0.881324
	β	0.557568	2.967028	2.409460	0.511531	2.787291	2.275760
	λ	0.837724	1.915286	1.077562	0.813002	1.841694	1.028692
350	α	0.967404	1.790023	0.822618	0.986293	1.783391	0.797098
	β	0.588115	2.802665	2.214550	0.555049	2.651643	2.096594
	λ	0.856122	1.837804	0.981682	0.836577	1.768651	0.932073
400	α	0.994199	1.777227	0.783028	1.011689	1.770162	0.758473
	β	0.596833	2.728179	2.131346	0.567673	2.587417	2.019743
	λ	0.863887	1.798504	0.934617	0.847195	1.736802	0.889606

The MCMC acceptance rates decrease from 0.5056 at $n = 50$ to 0.1872 at $n = 400$, while all 1000 Bayesian fits and corresponding credible intervals remain valid (Table 20).

For the illustrative sample, the MCMC diagnostics in Table 21 indicate large effective sample sizes, small MCSE-to-SD ratios, and $\widehat{R}$ values essentially equal to one. The corresponding upper confidence limits are also close to one (Table 22), supporting satisfactory MCMC convergence.

Prior sensitivity results are reported in Table 23. The posterior summaries remain broadly similar across the three Gamma prior specifications, although some variation is observed, particularly for β.

Table 20. Average MCMC acceptance rates in the second simulation setting.

n	Acceptance rate	Successful fits	Valid equal-tail intervals	Valid HPD intervals
50	0.505586	1000	1000	1000
150	0.324862	1000	1000	1000
250	0.248564	1000	1000	1000
350	0.203445	1000	1000	1000
400	0.187157	1000	1000	1000

Table 21. MCMC diagnostics for the illustrative sample under the second simulation setting.

Parameter	Posterior mean	Posterior SD	ESS	MCSE	MCSE/SD	Acceptance rate	$\widehat{R}$
α	1.496980	0.239111	3250.459	0.004194	0.017540	0.247617	1.000932
β	1.582989	0.690710	2500.935	0.013812	0.019996	0.247617	1.001256
λ	1.210040	0.280351	3278.122	0.004897	0.017466	0.247617	1.001072

Table 22. Upper confidence limits for the Gelman–Rubin diagnostic under the second simulation setting.

Parameter	$\widehat{R}$	Upper confidence limit
α	1.000932	1.002495
β	1.001256	1.003444
λ	1.001072	1.002870

Table 23. Prior sensitivity analysis for the illustrative sample under the second simulation setting.

Prior	Parameter	Posterior mean	Posterior SD	HPD lower	HPD upper	Acceptance rate
Gamma(2, 1)	α	1.490200	0.236056	1.044252	1.953824	0.252033
	β	1.586368	0.674345	0.310642	2.791386	0.252033
	λ	1.216368	0.275173	0.741293	1.755167	0.252033
Gamma(1, 0.5)	α	1.553494	0.267730	1.047495	2.061368	0.252067
	β	1.381889	0.776152	0.023735	2.698138	0.252067
	λ	1.141252	0.308046	0.631281	1.713222	0.252067
Gamma(0.5, 0.1)	α	1.566995	0.294763	0.981143	2.081988	0.257367
	β	1.340518	0.844336	0.007341	2.820622	0.257367
	λ	1.131591	0.338825	0.627056	1.806925	0.257367

Figure 8 displays the density, distribution, and hazard functions for the second parameter setting. Figure 9 shows the MSE behavior of the ML and Bayesian estimators as the sample size increases. Figure 10 shows stable MCMC traces and well-mixed posterior samples. Overall, the results show that increasing the sample size generally reduces estimation error and credible-interval length. The ML procedure exhibits high numerical convergence, while the Wald intervals provide lower coverage for β and λ. The Bayesian intervals show coverage closer to the nominal level for most settings, and the MCMC diagnostics indicate satisfactory convergence.

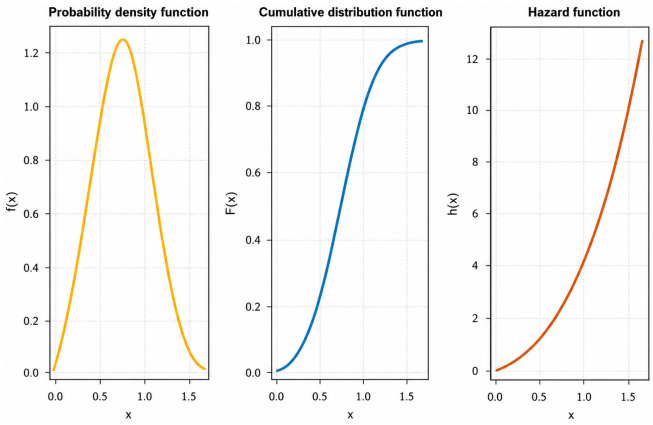


Figure 8. Probability density function, cumulative distribution function, and hazard function under the second parameter setting, $(\alpha, \beta, \lambda) = (1.5, 1.2, 1.1)$.

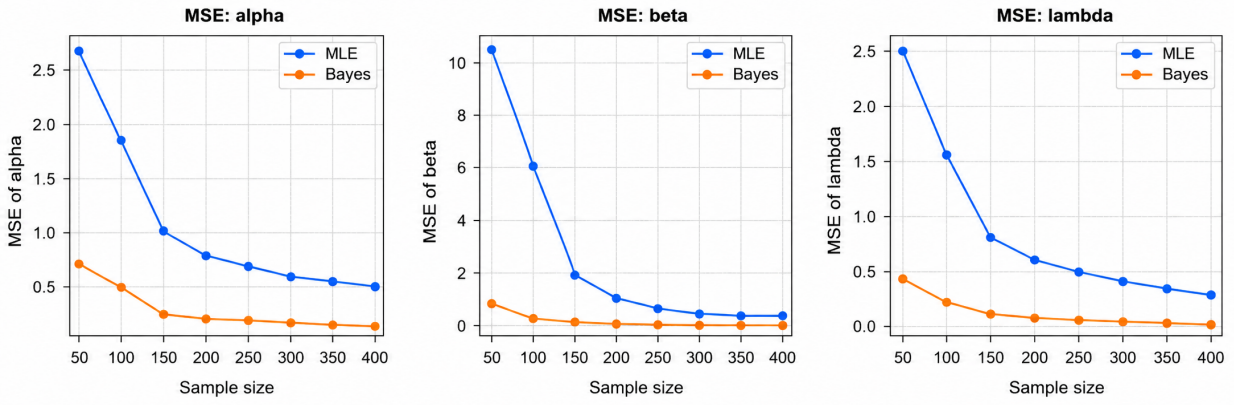


Figure 9. Comparison of the MSEs of the ML and Bayesian estimators under the second simulation setting.

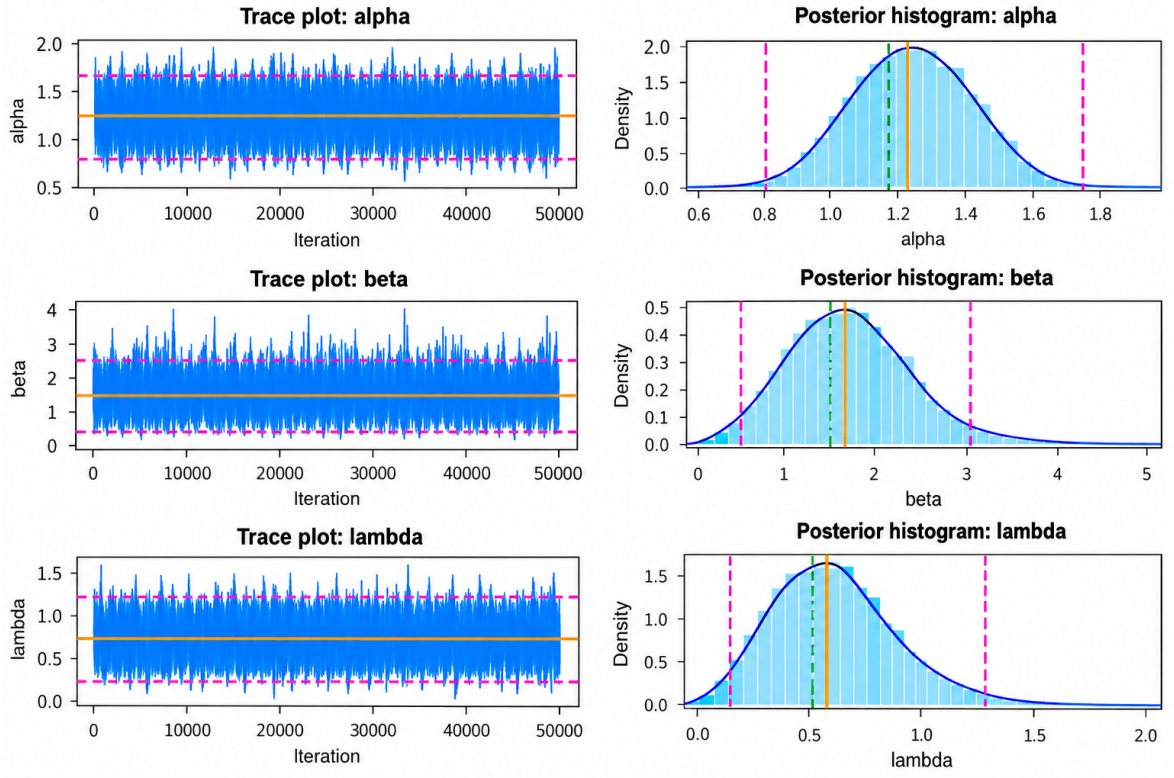


Figure 10. MCMC trace plots and posterior distributions for α, β, and λ under the second simulation setting.

6. Applications to real data

In this section, the practical performance of the proposed Kavya–Manoharan Cosine–Gompertz (KMCG) distribution is investigated using two real datasets. The proposed model is compared with several Gompertz-type competitors using maximum likelihood estimates, information criteria, goodness-of-fit statistics, parametric-bootstrap p-values, graphical diagnostics, and Bayesian inference.

6.1. Model comparison criteria

For a model with k parameters, sample size n, and maximized log-likelihood $\widehat{\ell}$, model comparison is based on the Akaike Information Criterion (AIC), Corrected Akaike Information Criterion (AICc), Bayesian Information Criterion (BIC), Consistent Akaike Information Criterion (CAIC), and Hannan–Quinn Information Criterion (HQIC), defined as

$$\mathrm{AIC} = -2\widehat{\ell} + 2k, \qquad \mathrm{BIC} = -2\widehat{\ell} + k\log n,$$

$$\mathrm{AICc} = \mathrm{AIC} + \frac{2k(k+1)}{n-k-1}, \qquad \mathrm{CAIC} = -2\widehat{\ell} + k(\log n + 1),$$

and

$$\mathrm{HQIC} = -2\widehat{\ell} + 2k\log(\log n).$$

Smaller values of these information criteria indicate a more favorable balance between model fit and complexity among the fitted models.

The Kolmogorov–Smirnov (KS), Anderson–Darling (AD), and Cramér–von Mises (CvM) statistics are also used to assess goodness of fit. In particular, the KS statistic is defined as

$$D = \sup_x \left| F_n(x) - F(x;\widehat{\boldsymbol{\theta}}) \right|,$$

where $F_n(x)$ denotes the empirical distribution function and $F(x;\widehat{\boldsymbol{\theta}})$ is the fitted distribution function. Smaller values of the KS, AD, and CvM statistics indicate closer agreement between the fitted model and the observed data. Since the model parameters are estimated from the same data used to compute the goodness-of-fit statistics, parametric-bootstrap p-values are additionally reported for the KS, AD, and CvM tests. These bootstrap p-values are used to assess the absolute adequacy of the fitted distributions rather than merely their relative performance.

In addition to the classical analysis, Bayesian estimation is performed for the proposed KMCG distribution and the competing models. Posterior means, posterior standard deviations, equal-tail and highest posterior density (HPD) credible intervals are reported. MCMC performance is examined using the effective sample size (ESS), Monte Carlo standard error (MCSE), the MCSE-to-posterior-standard-deviation ratio, acceptance rates, and the Gelman–Rubin $\widehat{R}$ diagnostic. Graphical comparisons of the fitted distributions and MCMC diagnostic plots are also provided to complement the numerical results.

6.2. Data Set 1: monthly real tax revenue in Egypt

The first dataset consists of monthly real tax revenue in Egypt, measured in units of 1000 million Egyptian pounds, from January 2006 to November 2010. The dataset, recently analyzed by [4], is used to evaluate the empirical performance of the proposed KMCG model. The observations are

5.9, 20.4, 14.9, 16.2, 17.2, 7.8, 6.1, 9.2, 10.2, 9.6, 13.3, 8.5, 21.6, 18.5, 5.1, 6.7, 17.0, 8.6, 9.7, 39.2, 35.7, 15.7, 9.7, 10.0, 4.1, 36.0, 8.5, 8.0, 9.2, 26.2, 21.9, 16.7, 21.3, 35.4, 14.3, 8.5, 10.6, 19.1, 20.5, 7.1, 7.7, 18.1, 16.5, 11.9, 7.0, 8.6, 12.5, 10.3, 11.2, 6.1, 8.4, 11.0, 11.6, 11.9, 5.2, 6.8, 8.9, 7.1, 10.8.

Table 24 summarizes the descriptive statistics of the monthly real tax revenue data.

Table 24. Descriptive statistics for the monthly real tax revenue data.

Sample size	Minimum	Maximum	Mean	Median	Std. deviation	Variance	Skewness	Kurtosis	CV (%)
59	4.1000	39.2000	13.4881	10.6000	8.0515	64.8266	1.5676	5.0793	59.69

A quantile–quantile (Q–Q) plot is used to compare the empirical quantiles with the corresponding theoretical quantiles of the normal distribution. Figure 11 presents the exploratory graphical analysis of the monthly real tax revenue data in Egypt, including the histogram with kernel density estimate, boxplot, empirical cumulative distribution function, normal Q–Q plot, density plot, and strip chart.

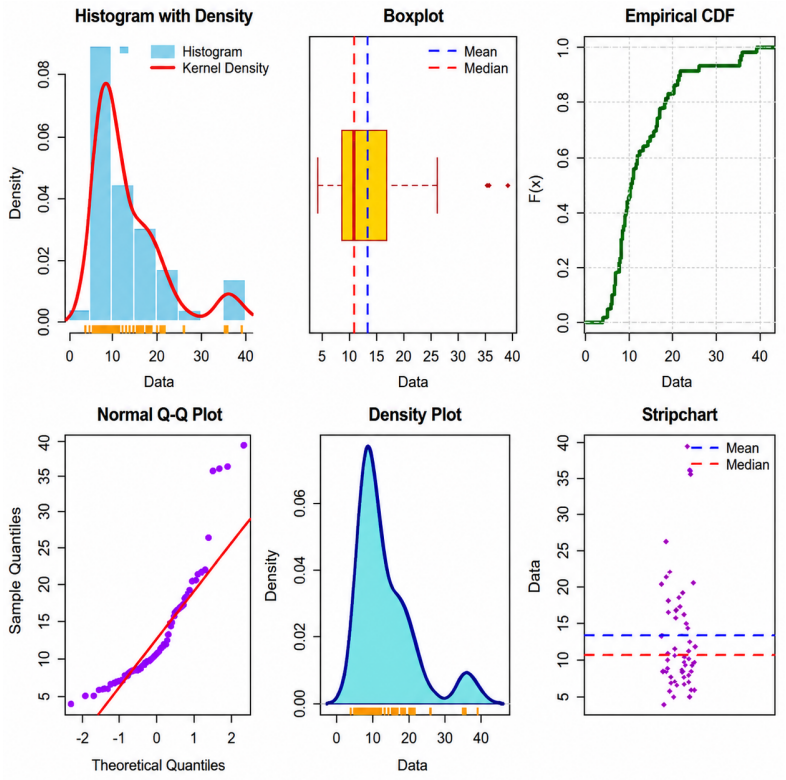


Figure 11. Exploratory graphical analysis of the monthly real tax revenue data in Egypt, including the histogram with kernel density estimate, boxplot, empirical cumulative distribution function, normal Q–Q plot, density plot, and strip chart.

Table 25 reports the maximum likelihood parameter estimates for the fitted models in Data Set 1.

Table 25. Maximum likelihood parameter estimates for Data Set 1.

Model	Parameter	Estimate
Proposed KMCG	α	0.0000017
	β	4.607707
	λ	0.196064
Cosine–Gompertz	β	0.028490
	λ	0.075984
Marshall–Olkin Gompertz	α	11.550687
	β	4.44155e-12
	λ	0.209164
Gompertz	α	0.053327
	λ	0.041003
Lindley	θ	0.139218
Inverse Gompertz	α	14.144635
	λ	3.530545
Transmuted Gompertz	α	0.023917
	λ	0.087710
	δ	-0.99999953

Bayesian credible intervals

The 95% equal-tail (ET) and highest posterior density (HPD) credible intervals are reported in Table 26.

Table 26. Bayesian equal-tail and HPD credible intervals for Data Set 1.

Model	Parameter	ET lower	ET upper	HPD lower	HPD upper
Proposed KMCG	α	1.03649e-08	2.88839e-07	3.79283e-10	2.43596e-07
Proposed KMCG	β	2.056771	7.127520	1.903205	6.942936
Proposed KMCG	λ	0.142823	0.238832	0.142974	0.238940
Cosine–Gompertz	β	0.007245	0.045288	0.006347	0.044049
Cosine–Gompertz	λ	0.058560	0.101005	0.057772	0.100059
Marshall–Olkin Gompertz	α	5.221841	23.081071	4.230361	21.050958
Marshall–Olkin Gompertz	β	1.42584e-09	2.89334e-08	2.02632e-10	2.44883e-08
Marshall–Olkin Gompertz	λ	0.155123	0.260511	0.154121	0.259220
Gompertz	α	0.026187	0.073513	0.027033	0.074066
Gompertz	λ	0.028069	0.061584	0.026736	0.059747
Lindley	θ	0.115329	0.165119	0.114769	0.164408
Inverse Gompertz	α	9.367231	17.827143	9.435532	17.880399
Inverse Gompertz	λ	2.249015	5.669866	2.066126	5.446771
Transmuted Gompertz	α	0.005906	0.041734	0.005084	0.040589
Transmuted Gompertz	λ	0.064676	0.111940	0.064524	0.111679
Transmuted Gompertz	δ	-0.998886	-0.691037	-0.999998	-0.756811

Table 27 lists the prior distributions specified for the Bayesian analysis of Data Set 1.

Table 27. Prior distributions used in the Bayesian analysis for Data Set 1.

Model	Parameter	Prior
Proposed KMCG	α	Gamma(2, rate = 19127800)
Proposed KMCG	β	Gamma(2, rate = 0.434055)
Proposed KMCG	λ	Gamma(2, rate = 10.2007)
Cosine–Gompertz	β	Gamma(2, rate = 70.2009)
Cosine–Gompertz	λ	Gamma(2, rate = 26.3213)
Marshall–Olkin Gompertz	α	Gamma(2, rate = 0.17315)
Marshall–Olkin Gompertz	β	Gamma(2, rate = 200000000)
Marshall–Olkin Gompertz	λ	Gamma(2, rate = 9.56186)
Gompertz	α	Gamma(2, rate = 37.5042)
Gompertz	λ	Gamma(2, rate = 48.7766)
Lindley	θ	Gamma(2, rate = 14.3659)
Inverse Gompertz	α	Gamma(2, rate = 0.141396)
Inverse Gompertz	λ	Gamma(2, rate = 0.566485)
Transmuted Gompertz	α	Gamma(2, rate = 83.6212)
Transmuted Gompertz	λ	Gamma(2, rate = 22.8023)
Transmuted Gompertz	δ	Uniform$(-1, 1)$

The numerical and graphical results for Data Set 1 provide a consistent comparison of the proposed KMCG distribution with the competing models. As shown in Table 28, the KMCG distribution yields the highest log-likelihood (−193.2925) and the lowest AIC (392.5851), AICc (393.0214), BIC (398.8177), CAIC (401.8177), and HQIC (395.0180) among the models considered. Thus, the improvement in likelihood remains favorable after accounting for model complexity. According to the information criteria, the Inverse Gompertz and Cosine–Gompertz distributions are the closest alternatives to the proposed model.

Table 28. Information-criterion comparison for Data Set 1.

Model	k	$\log L$	AIC	AICc	BIC	CAIC	HQIC
Proposed KMCG	3	-193.2925	392.5851	393.0214	398.8177	401.8177	395.0180
Inverse Gompertz	2	-196.2590	396.5180	396.7323	400.6731	402.6731	398.1400
Cosine–Gompertz	2	-196.7305	397.4610	397.6753	401.6161	403.6161	399.0830
Transmuted Gompertz	3	-196.9802	399.9604	400.3968	406.1930	409.1930	402.3934
Lindley	1	-200.6293	403.2586	403.3287	405.3361	406.3361	404.0696
Marshall–Olkin Gompertz	3	-198.8156	403.6313	404.0676	409.8639	412.8639	406.0642
Gompertz	2	-205.0142	414.0283	414.2426	418.1834	420.1834	415.6503

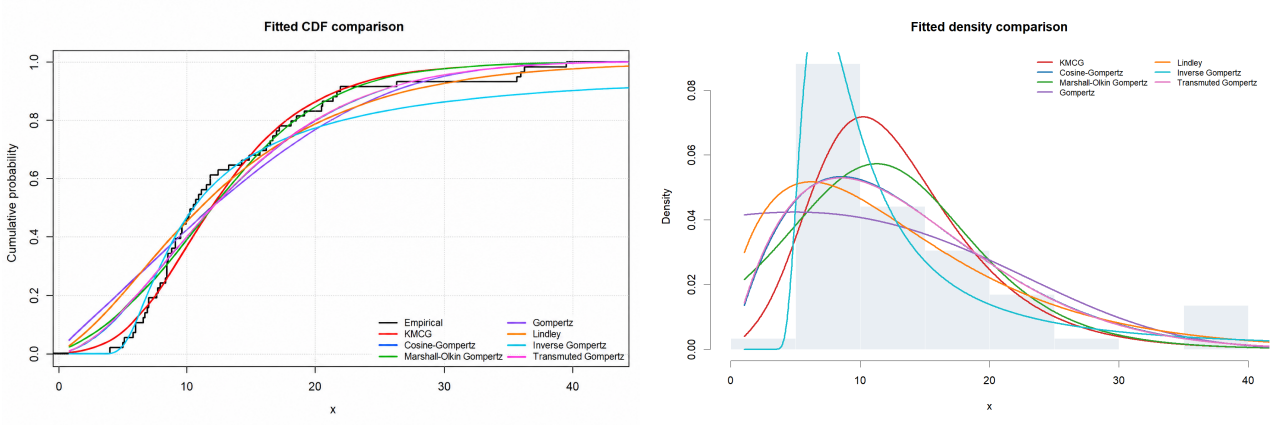
The goodness-of-fit results in Table 29 provide a similar, although more cautious, picture. The KMCG distribution has the smallest KS statistic (0.1182871) and AD statistic (1.1890362), whereas the Inverse Gompertz distribution gives a slightly smaller CvM statistic (0.1804852 compared with 0.1813718 for KMCG). However, the parametric bootstrap p-values are below 0.05 for all fitted models and all three goodness-of-fit statistics. Therefore, these results support the relative advantage of KMCG within the considered comparison set, but they also indicate that discrepancies between the fitted distributions and the observed data remain.

Table 29. Goodness-of-fit statistics and parametric bootstrap p-values for Data Set 1.

Model	KS	p_{KS}	AD	p_{AD}	CvM	p_{CvM}	B
Proposed KMCG	0.1182871	0.036	1.1890362	0.004	0.1813718	0.006	499
Cosine–Gompertz	0.1276401	0.020	1.7910767	0.002	0.2597305	0.002	499
Marshall–Olkin Gompertz	0.1246832	0.012	1.7580838	0.002	0.2293366	0.002	499
Gompertz	0.1966721	0.002	3.3941232	0.002	0.5298174	0.002	499
Lindley	0.1922164	0.002	2.9346004	0.002	0.4582272	0.002	499
Inverse Gompertz	0.1189772	0.018	1.1913008	0.012	0.1804852	0.026	499
Transmuted Gompertz	0.1309505	0.006	1.8206125	0.002	0.2625896	0.002	499

The graphical comparisons in Figure 12 complement these numerical findings. The fitted density curves show noticeable differences among the competing models, particularly in the location and height of the main density peak and in the representation of the right tail. The fitted CDFs similarly reveal model-dependent departures from the empirical distribution over different parts of the data range. The KMCG curve follows the main pattern of the empirical CDF reasonably closely over much of the observed range, which is consistent with its comparatively favorable information criteria and smaller KS and AD statistics. Nevertheless, visible local departures remain, in agreement with the small

bootstrap p-values. Hence, the graphical evidence should be interpreted as supporting the relative fit of KMCG among the models considered rather than as indicating an exact distributional fit.



(a) Fitted CDF comparison

(b) Fitted density comparison

Figure 12. Graphical comparison of the proposed KMCG distribution and the competing models for Data Set 1: (a) fitted density functions and (b) empirical and fitted cumulative distribution functions.

The Bayesian results in Tables 26 and 30 provide complementary estimates and interval summaries of parameter uncertainty. For KMCG, the posterior means of β and λ, 4.401977 and 0.191260, respectively, are reasonably close to their maximum likelihood estimates of 4.607707 and 0.196064. In contrast, the parameter α remains concentrated very close to zero, with an MLE of 0.0000017 and a posterior mean of 1.01506×10^{-7}. Its 95% equal-tail interval is $(1.03649\times10^{-8},\ 2.88839\times10^{-7})$, while the corresponding HPD interval is $(3.79283\times10^{-10},\ 2.43596\times10^{-7})$. This near-boundary behavior should be taken into account when interpreting the additional flexibility associated with this parameter.

Table 30. Bayesian parameter estimates for Data Set 1.

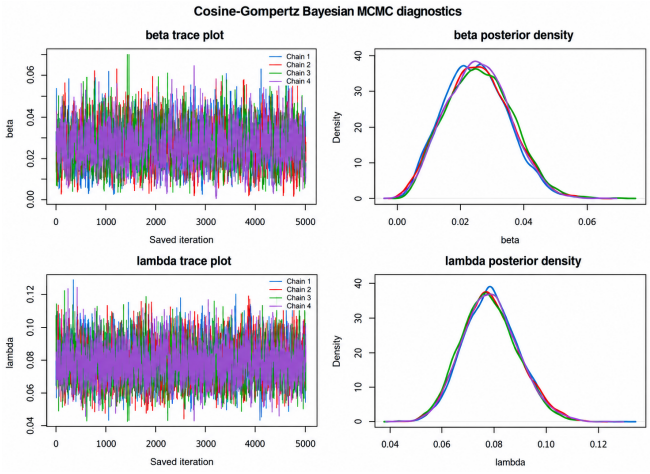
Model	Parameter	Posterior mean	Posterior SD
Proposed KMCG	α	1.01506e-07	7.41343e-08
	β	4.401977	1.280706
	λ	0.191260	0.024431
Cosine–Gompertz	β	0.025204	0.010045
	λ	0.078618	0.010817
Marshall–Olkin Gompertz	α	11.908820	4.567213
	β	1.03116e-08	7.33439e-09
	λ	0.206865	0.026633
Gompertz	α	0.050269	0.012062
	λ	0.042890	0.008579
Lindley	θ	0.139192	0.012714
Inverse Gompertz	α	13.682161	2.142452
	λ	3.733536	0.878949
Transmuted Gompertz	α	0.022456	0.009351
	λ	0.087293	0.012051
	δ	-0.920631	0.085167

The MCMC diagnostics reported in Table 31 and illustrated in Figures 13–15 provide further information on the Bayesian computations. Across the fitted models, the four chains generally overlap closely in the trace plots, without an evident persistent separation among chains, while the chain-specific posterior density curves show substantial agreement. This graphical behavior is consistent with the reported $\widehat{R}$ values, which are all close to one.

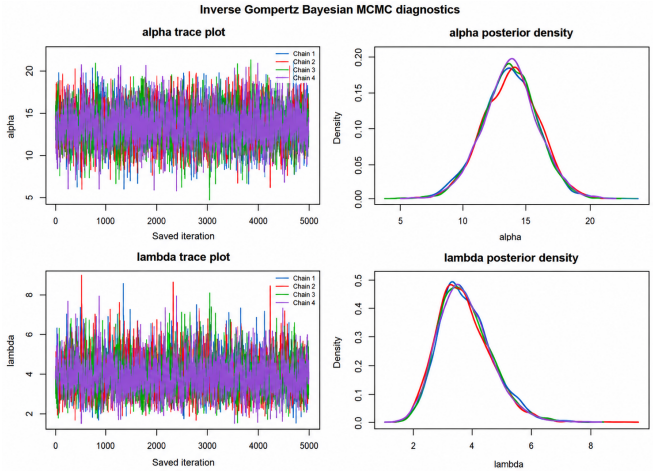
For the proposed KMCG model, the estimated $\widehat{R}$ values are 1.004832, 1.000099, and 0.999985 for α, β, and λ, respectively. The corresponding effective sample sizes are 374.84, 1835.67, and 2058.66. Thus, sampling efficiency is noticeably lower for α than for the other two KMCG parameters. In particular, the MCSE/SD ratio for α is 0.051651, compared with 0.023340 for β and 0.022040 for λ. This is also consistent with the trace and posterior-density plots for KMCG, where α is strongly concentrated near the boundary and displays a markedly right-skewed posterior distribution. The acceptance rate for the KMCG sampler is 0.436942, while the competing models have acceptance rates between approximately 0.43 and 0.46. For Data Set 1, KMCG provides favorable information-criterion values; however, it does not dominate all competitors according to every goodness-of-fit measure. In particular, the Inverse Gompertz distribution yields slightly smaller Anderson–Darling and Cramér–von Mises statistics. Therefore, the empirical evidence supports KMCG as a competitive model within the comparison set rather than establishing a general preference for KMCG over the Inverse Gompertz distribution. Overall, the numerical diagnostics and MCMC plots do not indicate a substantial between-chain convergence problem for the fitted models. However, the comparatively low ESS and larger MCSE/SD ratio for the KMCG α parameter indicate lower Monte Carlo precision for this parameter. Moreover, because its estimate is extremely close to the boundary and the Bayesian analysis uses the specified Gamma prior, inference concerning α should be interpreted cautiously. A prior-sensitivity assessment would therefore be useful for evaluating the robustness of the Bayesian conclusions concerning this parameter. Taken together, the information criteria, goodness-of-fit measures, fitted density and CDF plots, and Bayesian diagnostics suggest that KMCG provides a comparatively favorable representation of Data Set 1 within the models examined, while the bootstrap results and the near-boundary behavior of α warrant a cautious interpretation of the overall fit.

Table 31. MCMC convergence and efficiency diagnostics for Data Set 1.

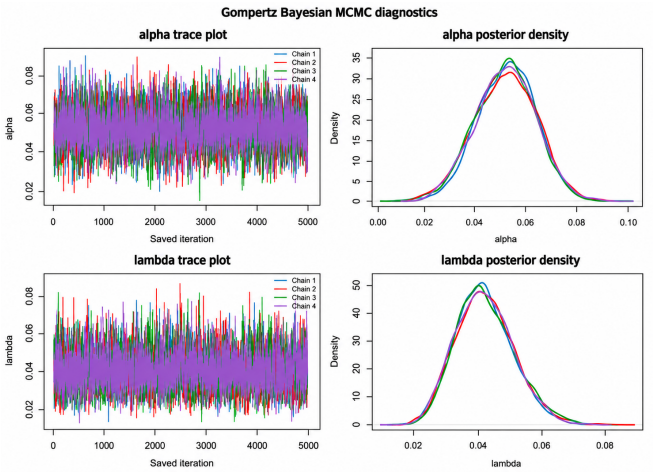
Model	Parameter	ESS	MCSE	MCSE/SD	$\widehat{R}$	Acceptance
Proposed KMCG	α	374.84	3.82911e-10	0.051651	1.004832	0.436942
Proposed KMCG	β	1835.67	0.029892	0.023340	1.000099	0.436942
Proposed KMCG	λ	2058.66	0.000538	0.022040	0.999985	0.436942
Cosine–Gompertz	β	2038.80	0.000222	0.022147	1.001267	0.433700
Cosine–Gompertz	λ	3539.21	0.000182	0.016809	1.000593	0.433700
Marshall–Olkin Gompertz	α	1501.22	0.117877	0.025809	1.000053	0.427758
Marshall–Olkin Gompertz	β	586.66	3.02811e-10	0.041286	1.001019	0.427758
Marshall–Olkin Gompertz	λ	1933.24	0.000606	0.022743	0.999996	0.427758
Gompertz	α	4001.65	0.000191	0.015808	1.000611	0.425117
Gompertz	λ	4667.08	0.000126	0.014638	1.000627	0.425117
Lindley	θ	16271.45	9.96677e-05	0.007839	0.999959	0.427700
Inverse Gompertz	α	3133.04	0.038276	0.017866	1.000361	0.442808
Inverse Gompertz	λ	2838.40	0.016498	0.018770	1.000447	0.442808
Transmuted Gompertz	α	1518.22	0.000240	0.025664	1.000913	0.459283
Transmuted Gompertz	λ	2517.49	0.000240	0.019930	1.000833	0.459283
Transmuted Gompertz	δ	1249.78	0.002409	0.028287	1.002486	0.459283



(a) Cosine–Gompertz

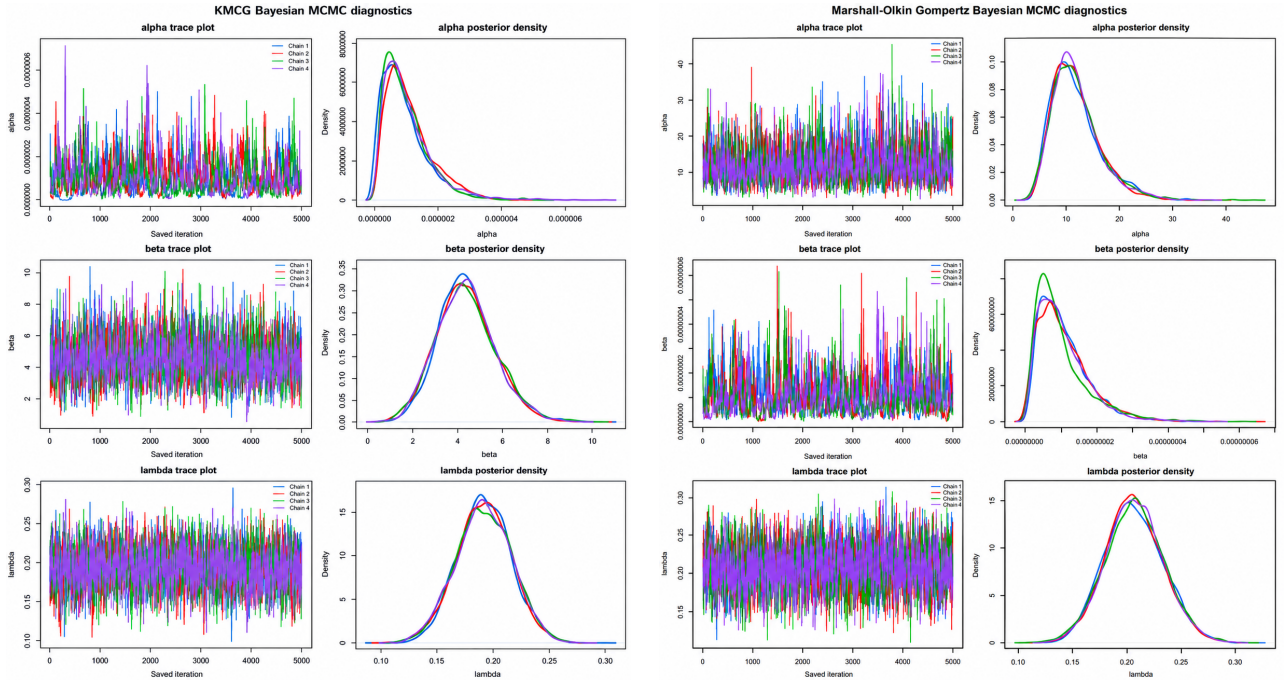


(b) Inverse Gompertz

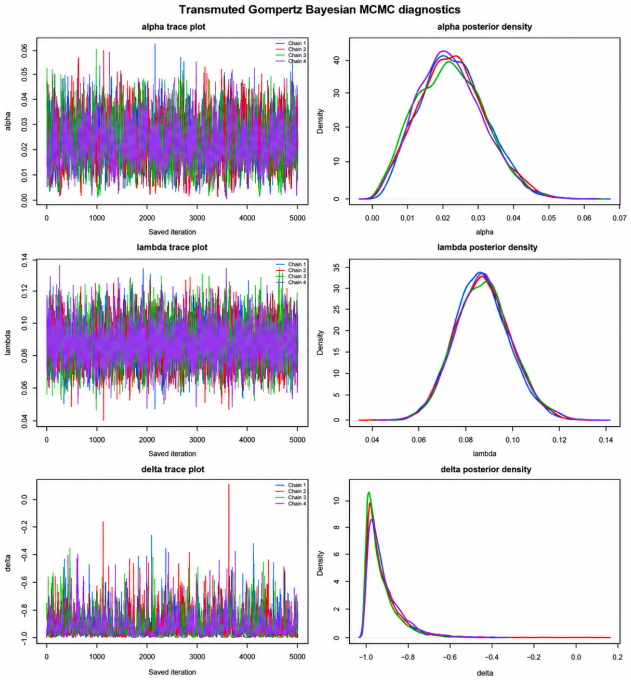


(c) Gompertz

Figure 13. MCMC trace plots and posterior density plots for the Cosine–Gompertz, Inverse Gompertz, and Gompertz models based on Data Set 1. The four MCMC chains are displayed separately.

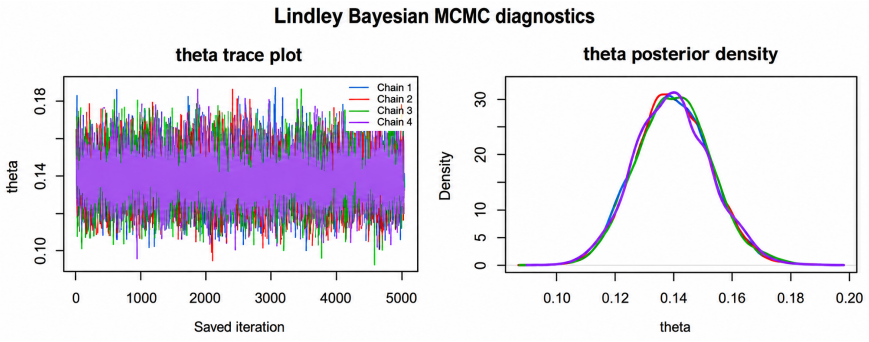


(a) Proposed KMCG **(b)** Marshall–Olkin Gompertz



(c) Transmuted Gompertz

Figure 14. MCMC trace plots and posterior density plots for the proposed KMCG, Marshall–Olkin Gompertz, and Transmuted Gompertz models based on Data Set 1. The four MCMC chains are displayed separately.



(a) Lindley

Figure 15. MCMC trace plot and posterior density plot for the Lindley model based on Data Set 1. The four MCMC chains are displayed separately.

6.3. Data Set 2: waiting times of bank clients

The second dataset contains the waiting times (minutes) of $n = 100$ bank clients and was originally analyzed by [10]. The observations are

0.8, 3.5, 4.9, 4.6, 10.7, 3.3, 13.0, 5.3, 10.9, 7.1, 6.9, 2.1, 17.3, 9.6, 21.4, 14.1, 4.4, 11.5, 12.9, 11.0, 8.9, 7.1, 4.7, 8.0, 13.7, 21.3, 1.3, 7.4, 9.7, 1.8, 7.1, 3.2, 3.6, 5.7, 6.2, 1.9, 4.0, 6.1, 4.7, 18.9, 19.0, 8.8, 5.5, 11.2, 4.4, 7.6, 13.3, 8.6, 4.1, 18.4, 4.2, 5.7, 38.5, 6.2, 8.6, 1.5, 8.9, 2.7, 1.9, 18.1, 21.9, 11.0, 7.7, 11.2, 7.1, 13.6, 13.1, 11.9, 18.2, 4.9, 19.9, 2.6, 20.6, 8.6, 9.8, 31.6, 11.1, 6.7, 8.8, 0.8, 4.3, 12.4, 4.8, 6.3, 23.0, 13.9, 2.9, 33.1, 8.2, 17.3, 15.4, 3.1, 5.0, 9.5, 12.5, 15.4, 4.2, 4.3, 27.0, 6.2.

The data range from 0.8 to 38.5 minutes. The mean (9.8770) exceeds the median (8.1000), while the skewness (1.4507) and kurtosis (5.4300) indicate positive skewness and a relatively heavy right tail.

Table 32 summarizes the main descriptive characteristics of Data Set 2. The sample consists of 100 observations ranging from 0.8000 to 38.5000 minutes, with a mean of 9.8770 and a median of 8.1000. The mean exceeding the median, together with the positive skewness coefficient of 1.4507, indicates a pronounced right-skewed distribution. The kurtosis value of 5.4300 further suggests relatively heavy tail behavior. These descriptive features motivate the use of flexible positively supported distributions for modeling the bank waiting-time data. Figure 16 provides a graphical assessment of the distributional characteristics of the bank waiting-time observations. The graphical pattern is consistent with the descriptive statistics in Table 32, particularly the positive skewness and the presence of a relatively long right tail. The concentration of observations at shorter waiting times, together with a smaller number of relatively large observations, indicates clear departure from symmetry and supports the consideration of flexible lifetime-type models for these data. Table 33 compares the fitted models according to the maximized log-likelihood and several information criteria. The proposed KMCG distribution has the highest log-likelihood, −317.1624, and the smallest AIC, AICc, BIC, CAIC, and HQIC values. The Transmuted Gompertz (TG) model follows very closely, with an AIC of 640.4535 compared with 640.3249 for KMCG. Thus, the AIC difference is only approximately 0.129, indicating that KMCG and TG have very similar empirical performance according to this criterion. Although KMCG attains the smallest information-criterion values among the models considered, the small

difference from TG does not support a claim of clear empirical superiority. Table 34 reports the maximum likelihood estimates for KMCG and the competing distributions. For KMCG, the estimates are $\widehat{\alpha} = 0.007835$, $\widehat{\beta} = 0.000120$, and $\widehat{\lambda} = 0.130594$. In particular, the estimate of β is very small and should be interpreted cautiously. Several competing models also contain parameters estimated close to their parameter-space boundaries. For example, the APG and PG estimates of α and the MOG estimate of β are close to zero, whereas the TG estimate $\widehat{\delta} = -0.999993$ lies very close to the lower boundary of its admissible range. These estimates indicate that boundary or near-boundary behavior is not restricted to the proposed model and should be considered when interpreting parameter estimates and subsequent inference.

Table 32. Descriptive statistics for the bank waiting-time dataset.

Sample size	Minimum	Maximum	Mean	Median	Std. deviation	Variance	Skewness	Kurtosis
100	0.8000	38.5000	9.8770	8.1000	7.2370	52.3741	1.4507	5.4300

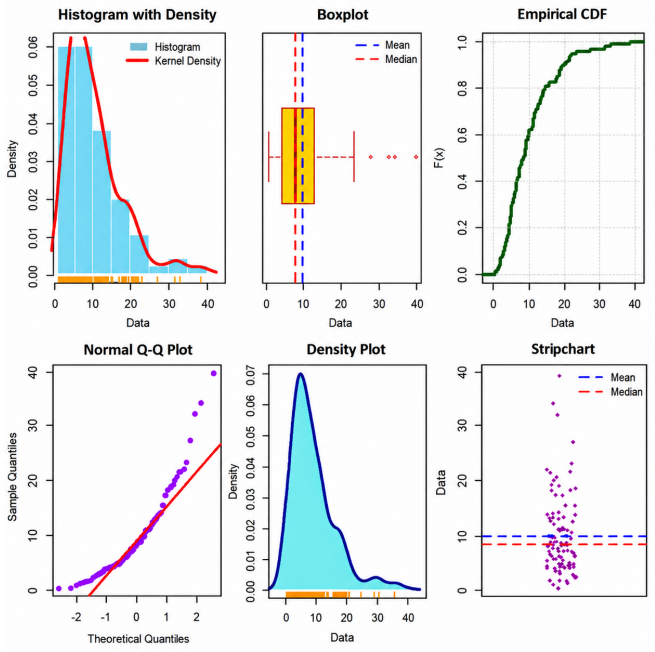


Figure 16. Exploratory graphical analysis of the bank clients' waiting-time data.

Table 33. Model selection criteria for Data Set 2.

Model	k	$\log L$	AIC	AICc	BIC	CAIC	HQIC
KMCG	3	-317.1624	640.3249	640.5749	648.1404	651.1404	643.4880
TG	3	-317.2267	640.4535	640.7035	648.2690	651.2690	643.6165
PG	3	-318.7307	643.4614	643.7114	651.2769	654.2769	646.6245
APG	3	-319.0368	644.0737	644.3237	651.8892	654.8892	647.2367
MOG	3	-320.7121	647.4241	647.6741	655.2396	658.2396	650.5872
G	2	-323.9756	651.9512	652.0749	657.1615	659.1615	654.0599
IG	2	-336.5585	677.1170	677.2407	682.3273	684.3273	679.2257

Table 34. Maximum likelihood estimates for Data Set 2.

Model	Parameter	Estimate
KMCG	α	0.007835
	β	0.000120
	λ	0.130594
APG	α	2.4238e-07
	λ	0.183068
	ρ	21.166330
IG	α	3.3085e-12
	λ	5.347602
PG	α	5.8345e-08
	β	1.458471
	λ	0.030461
MOG	α	4.116127
	β	2.8930e-07
	λ	0.192358
G	α	0.040799
	λ	0.071167
TG	α	0.002950
	λ	0.148497
	δ	-0.999993

Table 35 presents the KS, AD, and CvM goodness-of-fit statistics together with their parametric-bootstrap p-values. KMCG yields the smallest KS (0.041984), AD (0.153739), and CvM (0.021223) statistics among the fitted models. Its corresponding bootstrap p-values are 0.940, 0.976, and 0.952, respectively, providing no evidence against the fitted KMCG model at the 5% significance level. TG produces very similar results, with KS, AD, and CvM statistics of 0.042339, 0.160579, and 0.022351 and bootstrap p-values of 0.952, 0.966, and 0.952, respectively. APG, PG, and MOG are also not rejected at the 5% level. In contrast, the bootstrap p-values for Gompertz and Inverse Gompertz are below 0.05 for all three statistics, providing evidence of lack of fit for these two models. Thus, the goodness-of-fit results support KMCG as an adequate model while also showing that TG provides a closely comparable fit. Table 36 reports the Bayesian posterior means, posterior standard deviations, and 95% equal-tail credible intervals. For KMCG, the posterior means of α, β, and λ are 0.007273, 0.000119, and 0.131171, respectively. These values are close to the corresponding maximum likelihood estimates 0.007835, 0.000120, and 0.130594. The posterior standard deviations are 0.004505, 8.4477×10^{-5}, and 0.010796, respectively. Relative to their posterior means, α and especially the very small β parameter exhibit greater uncertainty than λ. Therefore, the Bayesian estimates are broadly consistent with the maximum likelihood results, although inference concerning the small KMCG shape parameters should be interpreted cautiously.

Table 35. Goodness-of-fit statistics and parametric bootstrap p-values for Data Set 2.

Model	KS	p_{KS}	AD	p_{AD}	CvM	p_{CvM}
KMCG	0.041984	0.940	0.153739	0.976	0.021223	0.952
APG	0.052857	0.664	0.376754	0.358	0.053937	0.378
IG	0.167454	0.002	3.999891	0.002	0.592359	0.002
PG	0.057791	0.542	0.405607	0.374	0.061030	0.370
MOG	0.059642	0.344	0.635123	0.074	0.076009	0.130
G	0.105975	0.006	1.627452	0.006	0.221397	0.004
TG	0.042339	0.952	0.160579	0.966	0.022351	0.952

Table 36. Bayesian estimates and 95% equal-tail credible intervals for Data Set 2.

Model	Parameter	Mean	SD	ET lower	ET upper
KMCG	α	0.007273	0.004505	0.000895	0.017901
	β	0.000119	8.4477e-05	1.5163e-05	0.000333
	λ	0.131171	0.010796	0.110533	0.153084
APG	α	2.6240e-07	1.7443e-07	3.3417e-08	7.0081e-07
	λ	0.182083	0.016619	0.148598	0.214498
	ρ	22.858698	10.956841	7.298213	49.548476
IG	α	1.0032e-08	7.0364e-09	1.4412e-09	2.7915e-08
	λ	5.344320	0.531238	4.359523	6.432983
PG	α	4.9509e-08	3.6415e-08	1.8007e-09	1.3828e-07
	β	1.458945	0.103381	1.236446	1.663606
	λ	0.031474	0.009221	0.016742	0.052051
MOG	α	4.158249	1.244622	2.230365	7.129493
	β	2.7833e-07	1.9656e-07	2.8199e-08	7.6693e-07
	λ	0.190267	0.023798	0.144785	0.238324
G	α	0.037737	0.011197	0.015274	0.059746
	λ	0.073406	0.010664	0.054104	0.095771
TG	α	0.002963	0.002106	0.000276	0.002859
	λ	0.143829	0.011907	0.120793	0.167250
	δ	-0.897089	0.094284	-0.996805	-0.652170

Table 37 presents the HPD credible intervals together with the prior distributions used in the Bayesian analysis. For KMCG, the HPD intervals are $(0.000713, 0.015744)$ for α, $(4.0468 \times 10^{-6}, 0.000286)$ for β, and $(0.109883, 0.152908)$ for λ. The interval for β remains concentrated at very small positive values, consistent with both its maximum likelihood estimate and posterior mean. The prior specifications also differ substantially across parameters and models. Consequently, the Bayesian results, particularly for parameters located close to zero, should be interpreted in conjunction with the adopted prior distributions. A prior-sensitivity assessment is especially relevant for the small KMCG β parameter.

Table 37. Highest posterior density intervals and prior distributions for Data Set 2.

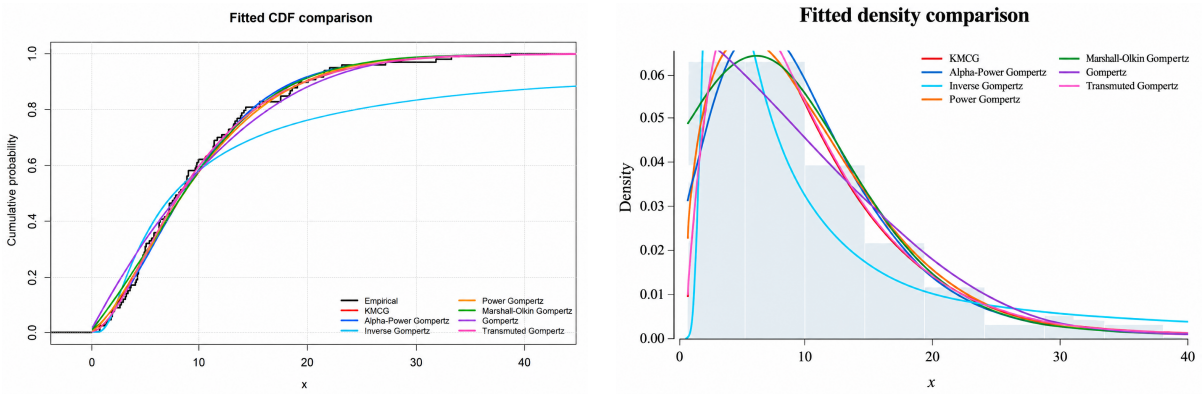
Model	Parameter	HPD lower	HPD upper	Prior
KMCG	α	0.000713	0.015744	Gamma(2, 255.278)
	β	4.0468e-06	0.000286	Gamma(2, 16598.7)
	λ	0.109883	0.152908	Gamma(2, 15.3146)
APG	α	1.7305e-08	6.0883e-07	Gamma(2, 8251570)
	λ	0.149756	0.215521	Gamma(2, 10.9249)
	ρ	4.961804	44.350728	Gamma(2, 0.0944897)
IG	α	4.3236e-10	2.3897e-08	Gamma(2, 200000000)
	λ	4.324189	6.388246	Gamma(2, 0.373999)
PG	α	3.1027e-10	1.1890e-07	Gamma(2, 34278600)
	β	1.259968	1.658835	Gamma(2, 1.3713)
	λ	0.015034	0.049422	Gamma(2, 65.6583)
MOG	α	2.003151	6.655141	Gamma(2, 0.485894)
	β	7.1621e-09	6.5990e-08	Gamma(2, 6913170)
	λ	0.144179	0.237673	Gamma(2, 10.3973)
G	α	0.015718	0.060091	Gamma(2, 49.0208)
	λ	0.053064	0.094404	Gamma(2, 28.103)
TG	α	8.4459e-06	0.007022	Gamma(2, 677.903)
	λ	0.120070	0.166292	Gamma(2, 13.4683)
	δ	-0.999984	-0.706449	Uniform$(-1, 1)$

Table 38 summarizes the MCMC convergence and efficiency diagnostics. For KMCG, the ESS values are 662.35, 622.86, and 3491.39 for α, β, and λ, respectively, while the corresponding MCSE/SD ratios are 0.038856, 0.040069, and 0.016924. Thus, the Monte Carlo standard errors correspond to approximately 1.7%–4.0% of the posterior standard deviations. The $\widehat{R}$ values of 1.002019, 1.001422, and 1.000204 are close to unity, and the reported acceptance rate is 0.463125. These results indicate reasonable convergence and Monte Carlo precision for the KMCG chains, although sampling efficiency is lower for α and β than for λ. Among the competing models, most $\widehat{R}$ values are likewise close to one; however, the PG parameter α has a comparatively small ESS of 89.28 and an MCSE/SD ratio of 0.105837, indicating less efficient sampling for that parameter.

Figure 17 complements the numerical goodness-of-fit results by comparing the fitted distribution and density functions with the empirical behavior of Data Set 2. The fitted KMCG curve follows the empirical distribution closely over the observed range. The competing curves, particularly TG, also show similar behavior over substantial parts of the data range. This graphical similarity is consistent with the small AIC difference between KMCG and TG and with their closely related goodness-of-fit statistics. Accordingly, the graphical evidence supports the adequacy of KMCG but does not indicate a pronounced separation from TG.

Table 38. MCMC convergence and efficiency diagnostics for Data Set 2.

Model	Parameter	ESS	MCSE	MCSE/SD	$\widehat{R}$	Acceptance
KMCG	α	662.35	0.000175	0.038856	1.002019	0.463125
	β	622.86	3.3849e-06	0.040069	1.001422	0.463125
	λ	3491.39	0.000183	0.016924	1.000204	0.463125
APG	α	584.28	7.2164e-09	0.041371	1.002782	0.441500
	λ	2098.06	0.000363	0.021832	1.000261	0.441500
	ρ	1111.82	0.328601	0.029990	1.000546	0.441500
IG	α	1183.99	2.0449e-10	0.029062	1.001266	0.423442
	λ	16586.84	0.004125	0.007765	1.000256	0.423442
PG	α	89.28	3.8539e-09	0.105837	1.008940	0.421167
	β	480.70	0.004715	0.045610	1.004049	0.421167
	λ	445.55	0.000437	0.047375	1.004254	0.421167
MOG	α	2159.16	0.026785	0.021521	1.001485	0.431283
	β	366.46	1.0268e-08	0.052238	1.004378	0.431283
	λ	2778.88	0.000451	0.018970	1.000651	0.431283
G	α	2393.37	0.000229	0.020441	1.000300	0.488333
	λ	3579.39	0.000178	0.016715	1.000079	0.488333
TG	α	540.32	9.0606e-05	0.043021	1.005666	0.470358
	λ	4602.79	0.000175	0.014739	1.000230	0.470358
	δ	1046.20	0.002915	0.030917	1.001128	0.470358



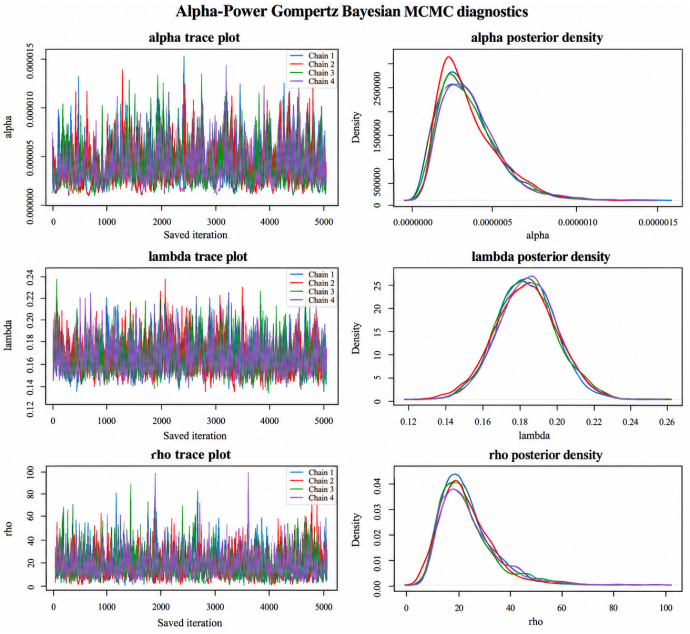
(a) Fitted CDF comparison

(b) Fitted density comparison

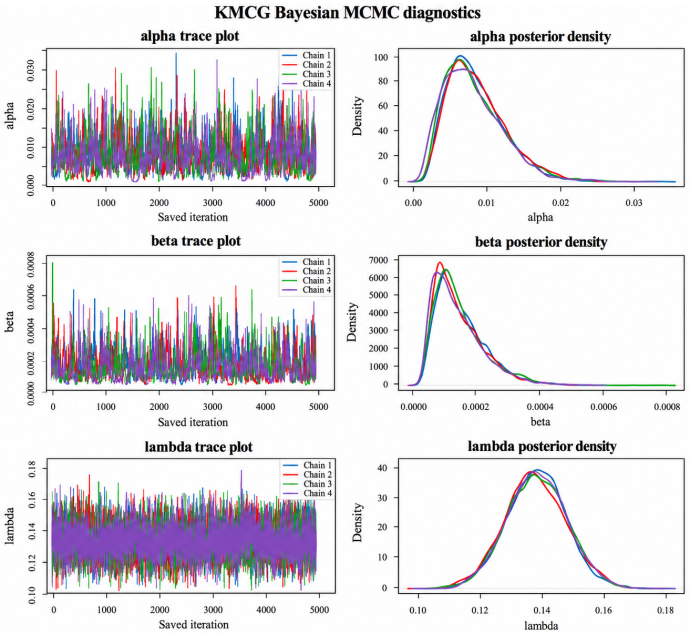
Figure 17. Graphical comparison of the proposed KMCG distribution and the competing models for Data Set 2: (a) empirical and fitted cumulative distribution functions and (b) fitted density functions.

Figure 18 displays the MCMC trace and posterior density plots for APG and KMCG. The trace plots provide a visual complement to the numerical convergence diagnostics reported in Table 38. For KMCG, the numerical $\widehat{R}$ values are close to one and the ESS values remain above 600 for all three parameters, with substantially greater ESS for λ. The posterior plots should therefore be interpreted together with these diagnostics, particularly for the relatively small α and β parameters. Figure 19 presents the MCMC trace and posterior density plots for the MOG, PG, and TG models. The corresponding $\widehat{R}$ values in Table 38 are generally close to one. Nevertheless, differences in effective

sample size indicate variation in sampling efficiency across parameters. This is particularly apparent for the PG α parameter, whose ESS is only 89.28 and whose MCSE/SD ratio is 0.105837. In comparison, TG has ESS values ranging from 540.32 to 4602.79, with $\widehat{R}$ values close to unity. The graphical and numerical diagnostics should therefore be considered jointly when assessing posterior simulation quality.

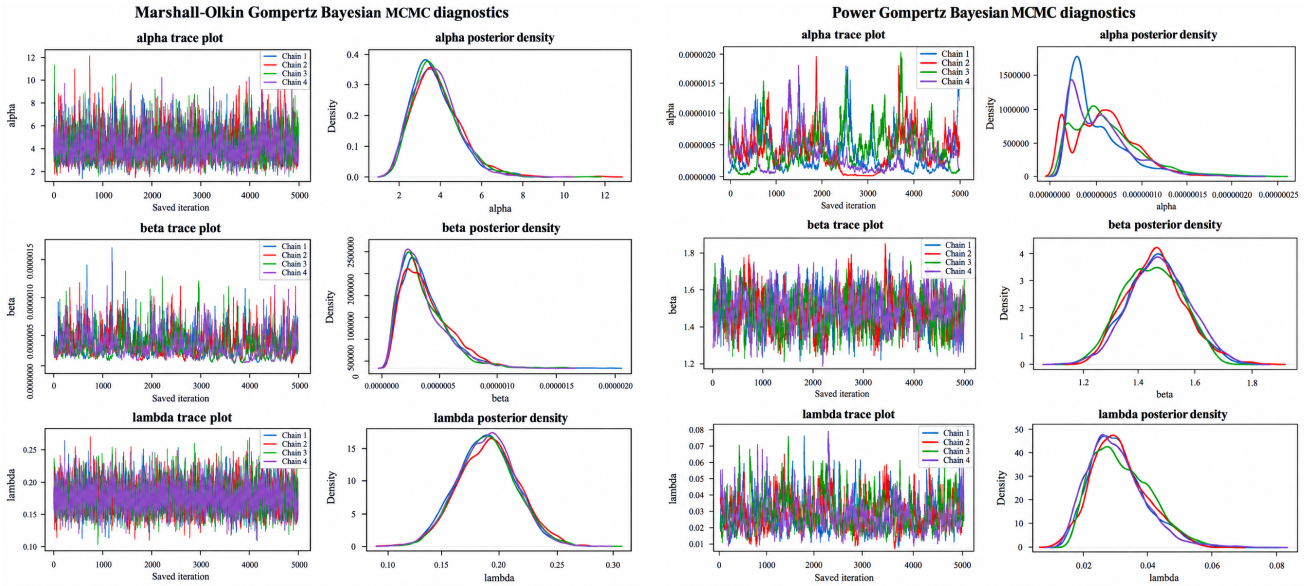


(a) Alpha–Power Gompertz

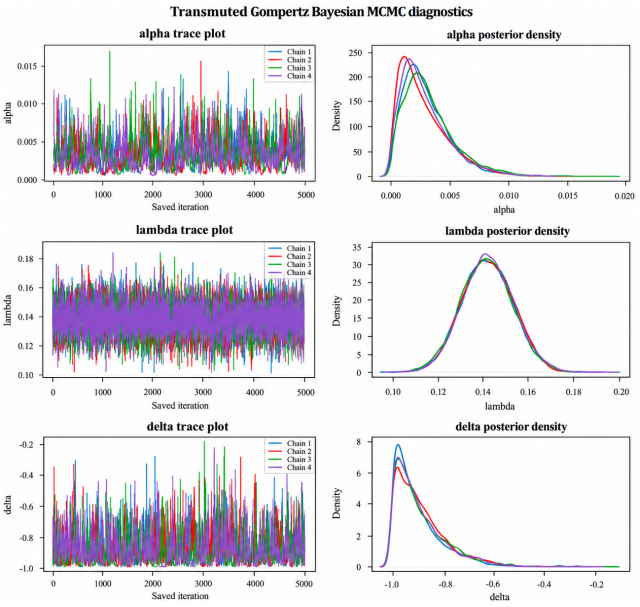


(b) Proposed KMCG

Figure 18. MCMC trace plots and posterior density plots for (a) the Alpha–Power Gompertz model and (b) the proposed KMCG model based on Data Set 2.



(a) Marshall–Olkin Gompertz **(b)** Power Gompertz

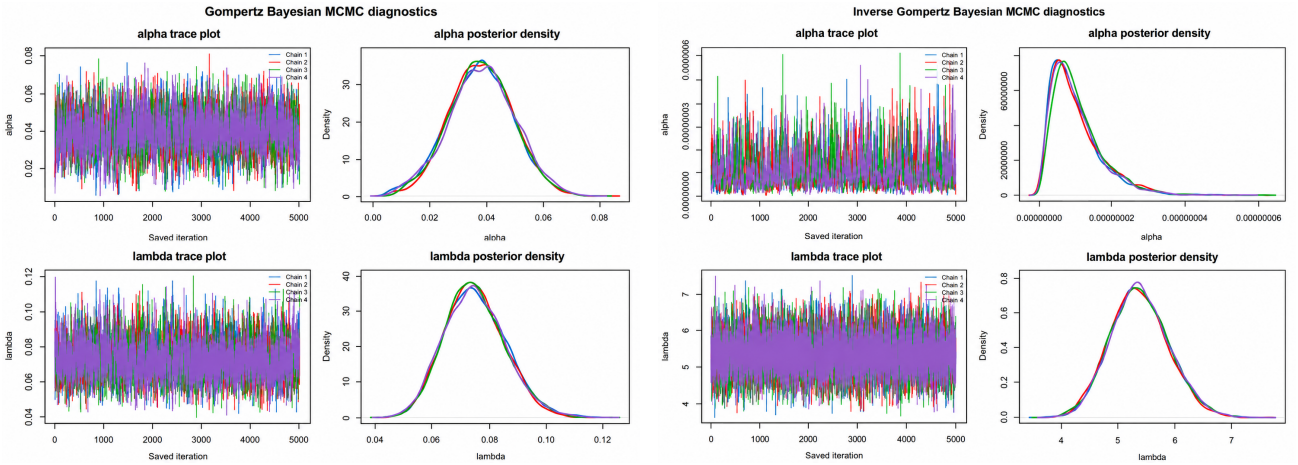


(c) Transmuted Gompertz

Figure 19. MCMC trace plots and posterior density plots for (a) the Marshall–Olkin Gompertz model, (b) the Power Gompertz model, and (c) the Transmuted Gompertz model based on Data Set 2.

Figure 20 shows the MCMC trace and posterior density plots for the Gompertz and Inverse Gompertz models. Their numerical MCMC diagnostics are favorable, with $\widehat{R}$ values close to one and relatively large effective sample sizes. Hence, the poor goodness-of-fit results obtained for these models cannot be attributed simply to evident MCMC convergence problems. Instead, the bootstrap results in Table 35 indicate that the Gompertz and Inverse Gompertz distributional forms do not adequately represent the observed waiting-time data despite satisfactory numerical MCMC

behavior. Overall, the numerical and graphical results provide a consistent but appropriately cautious assessment of the fitted models for Data Set 2. KMCG provides the highest log-likelihood and the lowest information criteria among the distributions considered. However, its AIC of 640.3249 differs from the TG value of 640.4535 by only approximately 0.129, indicating comparable empirical performance rather than a clear preference based on AIC alone. KMCG also yields the smallest KS, AD, and CvM statistics, with bootstrap p-values of 0.940, 0.976, and 0.952, respectively. These results reveal no significant discrepancy between the fitted KMCG distribution and the observations at the 5% level. APG, PG, MOG, and TG are also not rejected, whereas Gompertz and Inverse Gompertz show evidence of lack of fit according to all three bootstrap tests. The KMCG posterior means are close to the corresponding maximum likelihood estimates under the specified priors. Its credible intervals and posterior standard deviations indicate greater relative uncertainty in α and β than in λ, while the particularly small estimate of β warrants cautious interpretation and assessment of prior sensitivity. For KMCG, $\widehat{R}$ values are close to unity, ESS values range from approximately 623 to 3491, and MCSE values correspond to approximately 1.7%–4.0% of the posterior standard deviations, indicating reasonable MCMC performance. The fitted-function plots are consistent with the numerical results and show that KMCG closely represents the empirical behavior of the data, while TG provides a visually and numerically similar fit. Taken together, these findings support KMCG as a suitable candidate for modeling Data Set 2, while acknowledging the closely comparable empirical performance of the Transmuted Gompertz model and the uncertainty associated with the small KMCG shape parameters.



(a) Gompertz **(b)** Inverse Gompertz

Figure 20. MCMC trace plots and posterior density plots for (a) the Gompertz model and (b) the Inverse Gompertz model based on Data Set 2.

The near-boundary estimates observed for some KMCG parameters require careful interpretation. A parameter estimate close to zero, particularly when accompanied by substantial uncertainty, may indicate weak local identification or a relatively flat likelihood surface. However, a near-boundary estimate alone does not establish parameter redundancy or non-identifiability. A formal assessment would require additional likelihood-geometry analyses, such as profile-likelihood curves, likelihood contours, parameter-correlation analysis, and alternative parameterizations. Therefore, the present results are interpreted as evidence of possible weak identification rather than as proof of parameter

redundancy.

7. Conclusions

This study developed the Kavya–Manoharan Cosine–Gompertz (KMCG) distribution by applying the Kavya–Manoharan transformation to the Cosine–Gompertz distribution. The purpose of this construction was not to claim unrestricted distributional flexibility, but to obtain a three-parameter, relatively parsimonious Gompertz-type model with additional control over distributional shape while preserving an increasing hazard structure. The cumulative distribution, probability density, survival and hazard-rate functions, quantile function, moments, and order statistics were investigated to establish the principal mathematical and statistical characteristics of the model.

An important theoretical result is that the hazard-rate function is strictly increasing for all admissible values of $\alpha, \beta, \lambda > 0$. This property provides a clear interpretation of the scope of the proposed distribution. In particular, KMCG is appropriate when the underlying event-occurrence or failure mechanism can reasonably be represented by an increasing hazard. At the same time, this property constitutes an important limitation: the model cannot accommodate decreasing, bathtub-shaped, unimodal, or other non-monotone hazard-rate patterns. Consequently, the suitability of KMCG should be assessed in relation to the characteristics and substantive interpretation of the data rather than on the basis of flexibility claims alone.

Maximum likelihood and Bayesian procedures were considered for parameter estimation. The simulation results generally show reductions in estimation error and interval length as the sample size increases, supporting improved finite-sample estimation with larger samples. Bayesian estimation based on MCMC sampling produced estimates that were generally consistent with their maximum likelihood counterparts. Nevertheless, the simulation and real-data analyses also demonstrate that estimation can become more uncertain when shape parameters approach the boundary of the parameter space. Therefore, convergence diagnostics, Monte Carlo uncertainty, prior sensitivity, and parameter identifiability should be examined jointly rather than relying only on point estimates.

The two empirical applications illustrate that the relative performance of KMCG depends on both the dataset and the criterion used for comparison. For the Egyptian monthly real tax revenue data, KMCG provides favorable information-criterion values among the fitted models. However, it does not dominate every competitor according to every goodness-of-fit measure. In particular, the Inverse Gompertz distribution produces slightly smaller Anderson–Darling and Cramér–von Mises statistics than KMCG. Moreover, the KMCG estimate of α is extremely close to the boundary of its parameter space and is associated with substantial uncertainty. These findings indicate that the results for the first dataset should be interpreted as evidence of competitive performance rather than uniform empirical superiority. For the bank-client waiting-time data, KMCG attains the highest maximized log-likelihood and the smallest information-criterion values among the distributions considered. It also yields the smallest Kolmogorov–Smirnov, Anderson–Darling, and Cramér–von Mises statistics, with corresponding parametric-bootstrap p-values of 0.940, 0.976, and 0.952. Thus, there is no evidence against the fitted KMCG model at the 5% significance level according to these bootstrap tests. Nevertheless, the Akaike information criterion values for KMCG and the Transmuted Gompertz distribution are 640.3249 and 640.4535, respectively, giving a difference of only approximately 0.129. The two distributions therefore provide closely comparable empirical performance according to this

criterion, and the observed difference does not support a claim of pronounced superiority of KMCG. The very small estimate of the KMCG β parameter also requires cautious interpretation.

The near-boundary estimates observed in the empirical applications are an important limitation of the present analysis. Such behavior may be associated with weak parameter identification or a relatively flat likelihood surface in particular regions of the parameter space. Accordingly, the additional KMCG parameter should not automatically be interpreted as providing practically meaningful flexibility in every dataset. Profile-likelihood analysis, alternative parameterizations, and prior-sensitivity assessment are important complementary tools for distinguishing genuine parameter information from near-boundary or weakly identified behavior. Taken together, the theoretical, simulation, and empirical findings indicate that KMCG provides a useful additional three-parameter Gompertz-type model when an increasing hazard structure is appropriate. Its relatively parsimonious formulation is an attractive feature for model comparison, but parsimony alone does not establish better statistical performance. The empirical evidence obtained here is criterion and dataset dependent; hence, the proposed model should be viewed as a competitive alternative to, rather than a universal replacement for, existing Gompertz-type distributions.

Future research directions

The limitations identified in the present study suggest several directions for further investigation. A particularly important topic is parameter identifiability. The near-boundary estimates observed for α and β in the real-data applications motivate a more systematic examination of the likelihood geometry. Future studies may therefore investigate profile-likelihood curves, likelihood contours, parameter correlations, and alternative parameterizations to determine whether near-boundary behavior reflects weak identification, a flat likelihood surface, or genuine characteristics of the underlying data. Further Bayesian investigation is also warranted. In particular, posterior inference for weakly identified or near-boundary parameters may depend more strongly on prior specification. Future work may compare the Gamma priors considered here with weakly informative, diffuse, and objective prior specifications, including priors defined on transformed unconstrained parameter scales. Such comparisons would help distinguish information supplied by the likelihood from regularization introduced by the prior. Adaptive MCMC procedures and alternative posterior-sampling algorithms may also be investigated to improve sampling efficiency for parameters exhibiting relatively small effective sample sizes.

The simulation study may be extended by considering a broader range of parameter configurations, with particular emphasis on boundary and near-boundary cases motivated by the empirical applications. Larger sample sizes and additional Monte Carlo replications would permit a more detailed assessment of bias, root mean squared error, interval length, coverage probability, and the asymptotic behavior of the maximum likelihood and Bayesian estimators. Reporting Monte Carlo standard errors for estimated coverage probabilities would provide an additional measure of simulation uncertainty.

Alternative estimation methods, including maximum product spacing, ordinary and weighted least-squares estimation, percentile estimation, Cramér–von Mises estimation, Anderson–Darling estimation, and robust procedures, may also be investigated. Comparing these approaches under both regular and near-boundary parameter configurations could clarify whether alternative estimation techniques provide greater numerical stability than maximum likelihood estimation in weakly identified settings.

Future empirical studies should use a common and systematically selected set of recent Gompertz-type competitors across datasets whenever possible. Comparisons based on information criteria, goodness-of-fit statistics, parametric-bootstrap procedures, predictive performance, and graphical diagnostics would provide a more comprehensive assessment of the relative advantages and disadvantages of KMCG. Applications to larger and more diverse datasets would also help determine the conditions under which its additional shape parameter provides practically meaningful improvement. The KMCG model may additionally be extended to regression, frailty, cure-rate, stress–strength reliability, censoring, progressive censoring, and accelerated life-testing frameworks. These extensions would broaden its potential use in reliability and survival analysis. However, because the present KMCG distribution possesses a strictly increasing hazard rate, a separate methodological direction would be to develop related extensions capable of representing decreasing, bathtub-shaped, unimodal, or other non-monotone hazard patterns. Such developments would address one of the principal structural limitations of the current model and permit its underlying construction to be considered in a wider range of lifetime-data applications.

Author contributions

Conceptualization, F. B., A. M. K. and M. K.; methodology, F. B., A. M. K. and M. K.; formal analysis, F. B., A. M. K. and M. K.; investigation, F. B., A. M. K. and M. K.; software, F. B. and A. M. K.; validation, F. B., A. M. K. and M. K.; simulation study, F. B. and A. M. K.; Bayesian analysis, F. B. and A. M. K.; writing original draft preparation, F. B., A. M. K. and M. K.; writing review and editing, F. B., A. M. K. and M. K.; visualization, F. B. and A. M. K.; supervision, M. K. and F. B. All authors have read and agreed to the published version of the manuscript.

Use of Generative-AI tools declaration

The authors declare that no generative artificial intelligence (AI) tools were used in the preparation of this manuscript.

Acknowledgments

The authors are enormously grateful to the anonymous referees for their very careful reading of this paper and for their many valuable and detailed suggestions.

Conflict of interest

The authors declare that they have no financial or non-financial competing interests that could have influenced the work reported in this paper.

References

1. A. M. T. A. El-Bar, I. E. Ragab, On weighted exponential-Gompertz distribution: properties and application, *J. Taibah Univ. Sci.*, **13** (2019), 616–627. https://doi.org/10.1080/16583655.2019.1600277

2. M. M. Abdelwahab, A. B. Ghorbal, A. S. Hassan, M. Elgarhy, E. M. Almetwally, A. F. Hashem, Classical and Bayesian inference for the Kavya-Manoharan generalized exponential distribution under generalized progressively hybrid censored data, *Symmetry*, **15** (2023), 1193. https://doi.org/10.3390/sym15061193

3. F. M. A. Alam, On m X-Ray diffraction intensity using heavy-tailed probability distributions: a comparative study, *Crystals*, **15** (2025), 188. https://doi.org/10.3390/cryst15020188

4. S. Azam, M. Iqbal, M. Ali, M. Tabassum, B. Khalil, Semi modified alpha power rayleigh distribution: its properties and applications, *Res. Consort. Arch.*, **3** (2025), 706–721. Available from: `https://rcresearcharchive.com/index.php/Journal/article/view/234`.

5. D. Basalamah, T. Alballa, N. A. Noori, M. H. Jumaa, S. G. Nassr, Two-parameter Kavya–Manoharan cosine inverse Rayleigh distribution: statistical properties and application on radiation data, *J. Radiat. Res. Appl. Sci.*, **19** (2026), 102411. https://doi.org/10.1016/j.jrras.2026.102411

6. D. H. Castañeda, I. Cortés, Y. A. Iriarte, A Lambert-type Lindley distribution as an alternative for skewed unimodal positive data, *Mathematics*, **13** (2025), 3480. https://doi.org/10.3390/math13213480

7. J. T. Eghwerido, L. Nzei, I. J. David, O. D. Adubisi, The Gompertz extended generalized exponential distribution: properties and applications, *Commun. Fac. Sci. Univ. Ankara Ser. A1 Math. Stat.*, **69** (2020), 739–753. https://doi.org/10.31801/cfsuasmas.602930

8. J. T. Eghwerido, L. C. Nzei, F. I. Agu, The alpha power Gompertz distribution: characterization, properties, and applications, *Sankhya A*, **83** (2021), 449–475. https://doi.org/10.1007/s13171-020-00198-0

9. J. T. Eghwerido, F. I. Agu, The shifted Gompertz-G family of distributions: properties and applications, *Math. Slovaca*, **71** (2021), 1291–1308. https://doi.org/10.1515/ms-2021-0053

10. M. E. Ghitany, B. Atieh, S. Nadarajah, Lindley distribution and its application, *Math. Comput. Simul.*, **78** (2008), 493–506. https://doi.org/10.1016/j.matcom.2007.06.007

11. B. Gompertz, On the nature of the function expressive of the law of human mortality, and on a new mode of determining the value of life contingencies, *Phil. Trans. R. Soc. Lond.*, **115** (1825), 513–583. https://doi.org/10.1098/rstl.1825.0026

12. A. Hassan, A. M. Abdelghaffar, Bayesian and E-Bayesian estimation of Gompertz distribution in stress-strength reliability model under partially accelerated life testing, *Comput. J. Math. Stat. Sci.*, **4** (2025), 348–378. https://doi.org/10.21608/cjmss.2025.353923.1107

13. A. Hassan, A. Khalil, H. Nagy, Versatile extension of the unit Gompertz: efficient estimation and application, *Gazi Univ. J. Sci.*, **38** (2025), 1540–1564. https://doi.org/10.35378/gujs.1541941

14. A. M. Karakaş, F. Bulut, The New Gompertz distribution model and applications, *Symmetry*, **17** (2025), 843. https://doi.org/10.3390/sym17060843

15. A. M. Karakaş, F. Bulut, S. Çalık, A new Gompertz distribution for modeling tensile strength of carbon fibers and single carbon fibers data, *Mathematics*, **14** (2026), 2159. https://doi.org/10.3390/math14122159

16. A. M. Karakaş, F. Bulut, S. Şahin Bal, A novel Gompertz-type distribution with applications to radiological dose and pharmacokinetic data, *Mathematics*, **14** (2026), 702. https://doi.org/10.3390/math14040702

17. M. S. Khan, R. King, I. L. Hudson, Transmuted generalized Gompertz distribution with application, *J. Stat. Theory Appl.*, **16** (2017), 65–80. https://doi.org/10.2991/jsta.2017.16.1.6



AIMS Press

© 2026 the Author(s), licensee AIMS Press. This is an open access article distributed under the terms of the Creative Commons Attribution License (https://creativecommons.org/licenses/by/4.0)